SAND80-2137
Unlimited Release
UC-70

Eleana Near-Surface Heater Experiment Final Report

Allen R. Lappin, Robert K. Thomas, David F. McVey

Prepared by Sandia National Laboratories, Albuquerque, New Mexico 87185
and Livermore, California 94550 for the United States Department
of Energy under Contract DE-AC04-76DP00789

Printed April 1981

Sandia National Laboratories

2900-Q(3-80)

DISCLAIMER

Printed in the United States of America
Available from
National Technical Information Service
U. S. Department of Commerce
5285 Port Royal Road
Springfield, VA 22161

NTIS price codes
Printed copy: $6.00
Microfiche copy: A01

PAGES 1 to 2

WERE INTENTIONALLY

LEFT BLANK

SAND80-2137
Unlimited Release
Printed April 1981

Distribution
Category UC-70

Eleana Near-Surface Heater Experiment Final Report

Allen R. Lappin
Geological Projects Division 4537

Robert K. Thomas
Applied Mechanics Division I 5521

David F. McVey
Fluid Mechanics and Heat Transfer Division II 5512

Sandia National Laboratories
Albuquerque, NM 87185

Abstract

This report summarizes the results of a near-surface heater experiment operated at a depth of 23 m in argillite within the Eleana Formation on the Nevada Test Site (NTS). The test geometrically simulated emplacement of a single canister of High-Level Waste (HLW) and was operated at a power level of 2.5 kW for 21 days, followed by 3.8 kW to 250 days, when the power was turned off. Below 85° to 100°C, there was good agreement between modeled and measured thermal results in the rock and in the emplacement hole, except for transient transport of water in the heater hole. Above 100°C, modeled and measured thermal results increasingly diverged, indicating that the in-situ rock-mass thermal conductivity decreased as a result of dehydration more than expected on the basis of matrix properties. Correlation of thermomechanical modeling and field results suggests that this decrease was caused by strong coupling of thermal and mechanical behavior of the argillite at elevated temperatures.

No hole-wall decrepitation was observed in the experiment; this fact and the correlation of modeled and measured results at lower temperatures indicate that there is no *a priori* reason to eliminate argillaceous rocks from further consideration as a host rock for nuclear wastes. However, the phenomenological complexities apparent in the test, especially those related to rock-mass dehydration, make it obvious that additional in-situ testing must be done before shales can be adequately characterized for this purpose.

Acknowledgments

This report represents the final communication for a project some 3 years in duration. It incorporates the work of many people and involves conclusions and interpretations reached in many discussions. Special thanks, however, are due J. R. Cuderman, who initiated the fielding, and D. R. Waymire (4537/1116), who joined the project in the middle of initial fielding efforts and did an excellent job of continuing this work and of interfacing with fielding and instrumentation personnel.

Contents

Illustrations

Figure

Illustrations (cont)

Figure

Tables

Eleana Near-Surface Heater Experiment Final Report

Introduction

Argillaceous rocks, i.e., those rocks containing a major fraction of clay minerals, have long been considered a potential host medium for disposal of radioactive wastes. In 1957 the National Academy of Sciences considered shales appropriate for this purpose.[1] There are several apparent advantages to using argillaceous rocks:

1. Many argillaceous rocks, shales, and clay minerals are known to sorb a broad range of cations strongly.[2,3]
2. The in-situ permeability of many argillaceous rocks is very low.[4]
3. Most, but not all, shales are incapable of supporting open fractures at depth.[5,6]
4. Shales are largely insoluble.

Two major complexities are inherent in the effort to evaluate shales for waste management:

1. Shales are mineralogically complex, containing broadly varying proportions of quartz, clay minerals, carbonates, sulfides, and organic or carbonaceous material.
2. They contain appreciable volumes of water.

In addition, while much is known about some properties of argillaceous rocks, in other areas knowledge and experience are clearly inadequate. Only a few field tests have been operated in shales, to examine their thermomechanical response to emplacement of a heat source, and all have been conducted near-surface. Two tests were run in the Conasauga Formation of Tennessee,[7,8] and one in the Tertiary clays of southern Italy.[9] In addition, a test is under way in the Boom Clay of Belgium.

This report describes and summarizes the results of a near-surface heater test by Sandia National Laboratories in argillite from the Eleana Formation on the Nevada Test Site (NTS), Nevada (Figure 1), as part of the Nevada Nuclear Waste Storage Investigations (NNWSI). Detailed objectives of the report are to

1. Place the Eleana Near-Surface Heater Test in perspective as regards both test objectives and geologic setting
2. Describe the test geometry, instrumentation, and limitations
3. Describe the modeling studies made as part of the test evaluation
4. Describe experimental results and compare them with modeled behavior
5. Compare and contrast the results of this test with those of the Conasauga tests

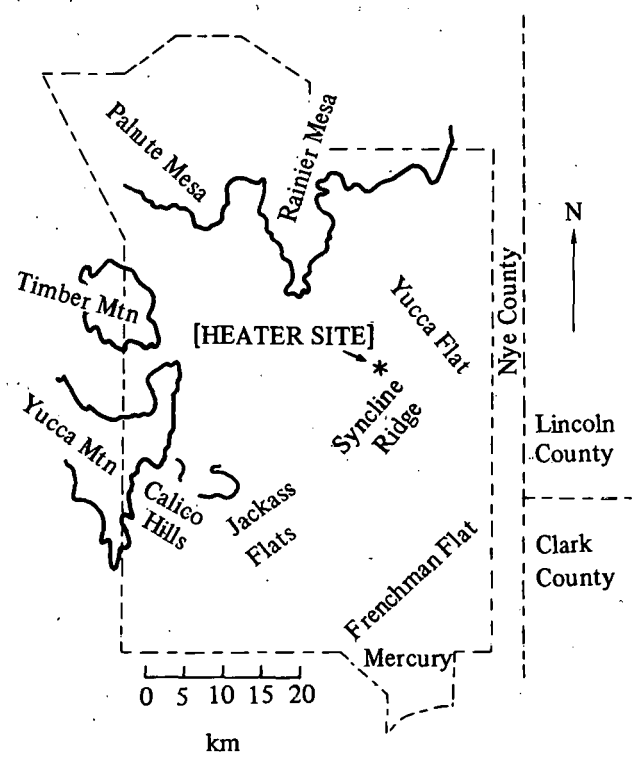

Figure 1. Index Map of Nevada Test Site (NTS)

Test Objectives

Because the Eleana Near-Surface Heater Test was the first field test in the Eleana Formation, its objectives were phenomenological and limited in scope, i.e., in most cases only qualitative information was sought, and only those objectives that could be addressed by instrumentation extending to the surface could be pursued. These objectives were to

1. Evaluate the possibility of compressive decrepitation of the heater-hole wall at power levels representative of those expected from a single conventional high-level waste (HLW) canister. Hole decrepitation was of concern because it might either decrease the in-situ thermal conductivity to the point where unacceptable temperatures resulted from constant-power operation or might mechanically hamper retrieval of the heater, and by inference, a waste canister.
2. Compare laboratory- and field-measured thermal responses of argillite in the Eleana Formation. This was of interest because only the in-situ response would include the effects of joints, inclined layering, and possible steam transport near the emplacement hole; the potential extent of these effects was unknown.
3. Identify phenomenological surprises—for example, how water contained in the rock would behave on heating.
4. Examine some of the instrumentation needs that would arise in a further effort to evaluate argillaceous rocks by means of in-situ tests.

Geology of the Eleana Formation

General

The Eleana Formation[10] is one of a series of laterally equivalent formations deposited during and as a result of the Antler Orogeny.[11] Rocks in this formation range from Upper Devonian to Lower Pennsylvanian in age, occur within an elongate trough extending from southern California to the Canadian border, and include a broad range of shales, argillites, siltstones, sandstones, conglomerates, and limestones. Although the Eleana Formation itself is defined over only a limited area,[10] equivalent rocks occur widely in Nevada and Utah.[12]

Syncline Ridge

Within the area on and near NTS, the Eleana Formation outcrops abundantly. In the Syncline Ridge area (see Figures 1 and 2), two structural blocks, possibly of repository size, are underlain by thick sections of the Eleana Formation.[13] For this reason, a program was launched in FY 1976 to investigate the feasibility of emplacing nuclear wastes in the Eleana Formation on NTS, with major emphasis on Syncline Ridge.

On NTS, the Eleana Formation is subdivided into ten units designated A through J (from the bottom up), and totaling some 3000 m or more in thickness.[11,13] Of the various units, units A through D, F, and G are predominantly quartzites and conglomerates, and contain only minor argillite and limestone. Subunit I is made up of thin-bedded limestones.

Units E, H, G, and J are predominantly argillite, a fine-grained metamorphic equivalent of siltstone or shale. High-quartz argillites are metamorphosed siltstones, while high-clay argillites (argillaceous argillite) are metamorphosed shales. In general, argillite in these units is highly siliceous and relatively low in clays, apparently because of its derivation from Paleozoic cherts to the west.[13] The major exception is the uppermost unit of the Eleana, Unit J. It is this unit that underlies most of the Syncline Ridge area of NTS and is dealt with in the rest of this report.

As part of the exploration program in argillite, Drillhole UE17e was drilled on the west flank of Syncline Ridge during early FY 1977.[14] Hole UE17e is within 100 m of the near-surface experiment described here. In UE17e, the first 74 m of drilling encountered a quartzite subunit of high- and low-quartz argillites interbedded with limestones, siltstones, and quartzites. From a depth of 74 to 914 m (the total depth), the hole was in the argillite subunit of Unit J. This subunit is made up of more than 99% argillite and contains only a very few minor quartzite beds.[14]

The overall mineral assemblage of argillite from Hole UE17e was:

quartz + "illite" +/- kaolinite (chamosite) +/- pyrophyllite +/- siderite +/- chlorite +/- plagioclase +/- potassium feldspar +/- pyrite +/- calcite +/- vermiculite.[15,16]

Quartz contents of 15 samples, as determined by X-ray analysis, ranged from a low of 15 to a high of 48 wt%.[17] Based on these results, Hodson and Hoover arbitrarily distinguished between high- and low-quartz argillite at 25 wt% quartz. Using this criterion, they reported that 80% of the argillite in UE17e was high-quartz, and 20% is low-quartz.

In almost all samples, the dominant clay mineral was a poorly crystalline mixed-layer clay, as indicated by the tracings in Figure 3. The 001 (basal) peak of the illite was generally at a spacing of 10.2 Å to 10.4 Å. The peak was lowered and shifted to lower basal spacing by treatment with ethylene glycol, because of interaction of the 001 reflection of illite with the 002 (~8.5 Å) reflection of expanded montmorillonite. Heating of samples at 400°C for 24 hours resulted in marked sharpening and increased height of the basal peak at a spacing of 9.9 Å to 10.1 Å, which suggests

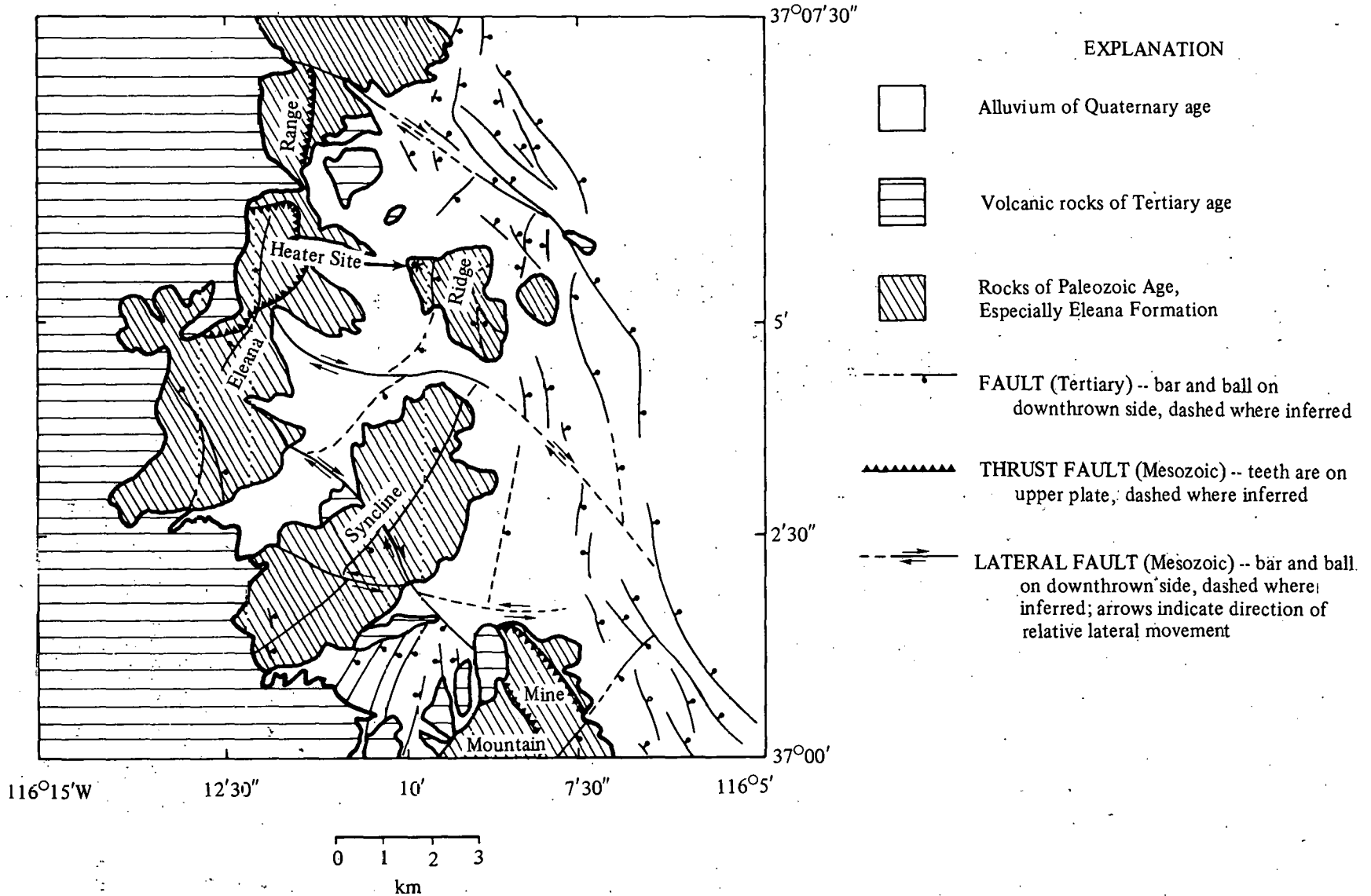

Figure 2. Geologic Map of the Syncline Ridge Region (Geology simplified from Reference 13)

that the mixed-layer illite in the Eleana contains variable amounts of expandable phase. Since the basal spacing also varied after heating, the illite apparently often includes chloritic material as well.

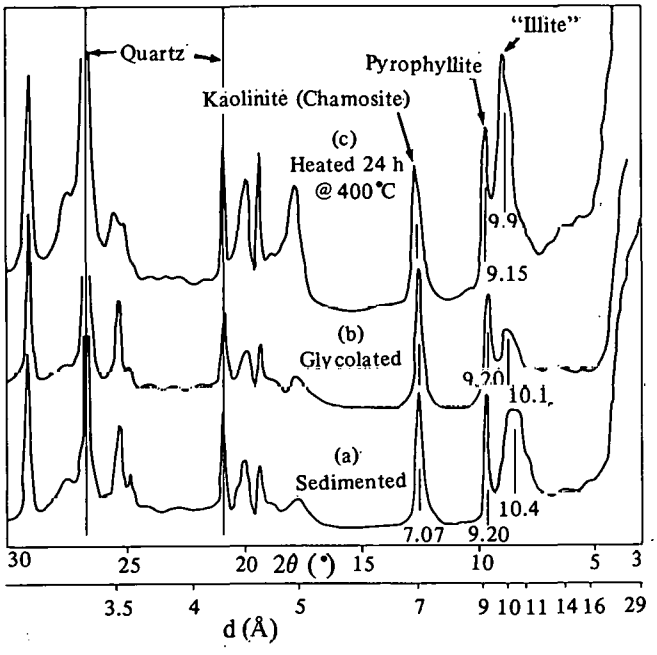

Figure 3. X-Ray Powder Diffraction Results, Sample UE17e-3000 (The three curves are normalized to the quartz peaks at 4.26 and 3.34 Å)

Many samples appeared to contain the septochlorite chamosite, as well as kaolinite. This interpretation is based on the frequent position of a broad 7 Å peak at slightly lower °2θ than would be expected for kaolinite alone, coupled with the fact that peaks were often present at the 002 positions for both kaolinite (3.58 Å) and chamosite (3.51 Å to 3.53 Å). The presence of chamosite is consistent with the widespread presence of siderite, ($FeCO_3$), generally the dominant or only carbonate present.

Pyrophyllite was quite common in samples from the lower part of UE17e. This phase, which indicates at least local instability of the assemblage kaolinite plus quartz, is common in many of the Paleozoic "shales" of Nevada and Utah.[18,19] The basal spacing of the pyrophyllite in UE17e generally exceeded the textbook value; it was from 9.2 Å to 9.4 Å, rather than from 9.14 Å to 9.21 Å (see Figure 3). Based on the very small shifts in 001 peak position on heating, it is concluded that any rectorite-type interlayering in the pyrophyllite is quite minor.

The Eleana argillite from Hole UE17e also contains appreciable amounts of carbonaceous material.[20] Table 1 presents the results of carbon analyses of 10 samples from depths of between 472 and 914 m. The argillite frequently contained ~0.5 wt% organic carbon, as verified by qualitative gas chromatograph-mass spectrometer scans in which heavy organics were consistently evolved at temperatures above 100° to 150°C. Secondly, the similarity between total carbon contents at 1000° and 1500°C indicates that there is no well-crystallized or pyrolitic graphite in the Eleana; however, the average difference of 0.9 wt% between total carbon contents measured at these temperatures and at 500°C indicates that partially or poorly crystallized graphitic material was generally present. This is apparently responsible for the strong sorption of technetium (Tc) exhibited by some argillite.[21]

Table 1. Carbon Analyses of Argillite From the Eleana Formation, Hole UE17e, NTS (Data from Reference 20.)

Analysis Temperature (°C)	Type of Carbon Measured	wt% (average 10 samples)	Standard Deviation (wt%)
80	Mineral carbon, evaluated by CO_2 evolution	0.48	0.27
500	Organic carbon, may include slight relict mineral carbon	0.49	0.11
1000	Total carbon, *except* pyrolitic graphite, if present	1.83	0.38
1500	Total carbon, including pyrolitic graphite	1.87	0.36

Chemical analyses of several samples of Eleana, both from Hole UE17e and from the heater site, are compiled and compared with compositions of other argillaceous rocks in Table 2. The alumina content of analyzed samples from the Eleana was higher than for all other rock types except residual clay. Because of the presence of siderite, the Fe_2O_3/FeO ratio was lower than for any other rock type. The Eleana's content of potentially leachable cations such as Mg, Ca, Na, and K is lower than for any other rock type except residual clay. It thus appears that the bulk composition of argillite from the Eleana Formation is transitional between that of representative normal shales and that of a residual clay. This fact almost certainly reflects the provenance of the formation; i.e., its derivation from first- and/or second-generation silicic rocks to the west.

Trace-element data for the Eleana are given in Table 3 and compared with data for average shales and the Pierre Formation. Except for Ba and Cl, the trace-element contents of both the at-depth and the near-surface Eleana appear to be within the range for other argillaceous rocks. The Eleana's markedly lower content of Cl would appear explainable by its metamorphism and resultant depletion of pore-water Cl.[29]

Fracturing and jointing are pervasive in Hole UE17e.[14] The majority of fractures are subparallel to the bedding, which dips between 12° and 80°. Fracture frequencies range from 3.4 to 9.4/m in the upper 153 m of cored interval. In the lower portion of the hole, fracture frequency ranges from 1.4 to 5.9/m, averaging 3.5. In general, sections of predominantly high-quartz argillite have lower fracture frequencies than those that are mainly low-quartz argillite (argillaceous argillite). Portions of the high-quartz argillite might be competent for construction purposes; the bulk of the argillaceous argillite would not.[14]

Syncline Ridge has been affected by Paleozoic, Mesozoic, and Tertiary deformations.[13] Paleozoic deformations, too large in scale to be evident over such a small area, are related to periodic deformations and shifts in the position of the axis of the Antler Foredeep.[11] Mesozoic deformation appears responsible not only for the major folding, thrust faulting, and lateral faulting, but also for some highly inclined faulting (see Figure 2). Relatively minor Tertiary faults (largely normal) form the eastern boundary of the area, and lie near or just beyond other boundaries of defined structural blocks.[13] It is in part this complexity, which became apparent in structural and geophysical investigations,[30] that caused deferral of further exploratory activity in the Syncline Ridge area.

Heater Site

As shown in Figure 1, the site for the Eleana Near-Surface Heater Experiment was on the western flanks of Syncline Ridge. The experiment was vertically emplaced at a heater center-plane depth of 22.9 m.

The experimental site is capped by thin-bedded quartzites ~5 m thick; these quartzites are underlain to a depth of 16 m[31] by a gradational unit of quartzite, siltstone, claystone, and argillite. This capping by quartzites probably accounts for the fact that obvious macroscopic iron staining of the argillite at the heater site extends to a depth of only 16 to 17 m; argillite at other locations is weathered to much greater depths. The lower limit of this staining was used to determine a minimum experiment depth, since it approximately delineates the depth where groundwaters are no longer strongly oxidizing. In fact, the mineralogy of samples from the near-surface instrumentation holes was indistinguishable from that of samples collected at depth in Hole UE17e, except that pyrophyllite and pyrite were absent in the shallow holes. Pyrophyllite was also absent in other relatively shallow holes in the area, as well as in Hole UE1*l*, which extended to a depth of 1524 m. Its absence may be controlled by either stratigraphic compositional variations or by near-surface weathering. The absence of pyrite appears to indicate that, although downward-moving groundwaters no longer precipitate iron oxides at the depth of the experiment, they are still oxidizing enough to make pyrite unstable.

From a mechanical point of view, argillite from the lower portions of the experimental holes is similar to that from the upper portion of Hole UE17e. The predominant joint orientation is subparallel to bedding, which dips to the southeast at about 30°.

Test Geometry and Instrumentation

Figure 4 shows drill-hole locations for the heater experiment. A 6 x 7.3 m concrete pad was poured over the site, and drill collars set before drilling. All drill holes were cased and cemented to a depth of 18 m. The holes were first drilled to casing depth and casings cemented in place. After the grout set, the holes were extended to nominal depth. The uncased portions of drill holes were carefully sealed from water migration through the obviously weathered zone. This procedure did not prevent penetration of surface waters to experiment depths presumably because at least some joints remained open to depths below the bottom of the casing.

Table 2. Bulk Chemical Analyses of Argillaceous Rocks (Wt%) (Argillite from Eleana Formation)

Oxide	Hole UE17e[22] Average (8 samples)	Hole UE17e[22] Standard Deviation	Heater Site[23] Average (5 samples)	Heater Site[23] Standard Deviation	Average Paleozoic Shale[24] (51 samples)	Residual Clay[24] on Norton Gneiss	Pierre Shale (232 Samples)[25] Average	Pierre Shale (232 Samples)[25] Standard Deviation
SiO_2	58.33	3.73	59.48	1.65	60.15	55.07	60.8	7.9
Al_2O_3	20.20	3.67	19.40	1.05	16.45	26.14	14.4	2.5
Fe_2O_3	0.75	0.34	0.77	0.15	4.04	3.72	3.4	1.4
FeO	4.92	1.58	3.99	0.31	2.90	2.53	1.1	1.2
MgO	1.79	0.26	1.35	0.06	2.32	0.33	2.2	1.0
CaO	0.70	0.28	0.80	0.05	1.41	0.16	2.6	0.45
Na_2O	0.89	0.19	0.33	0.01	1.01	0.05	1.1	0.56
K_2O	1.49	0.36	1.44	0.08	3.60	0.14	2.4	0.57
$M_gO+C_aO+K_2O+Na_2O$	4.87	--	3.92	--	8.34	0.68	8.3	--
H_2O+CO_2 (tot)	9.49	0.96	10.88	0.38	6.17	10.75	7.50[a]	1.77
TiO_2	0.85	0.07	0.89	0.16	0.76	1.03	0.58	0.12
P_2O_5	0.26	0.06	0.20	0.01	0.15	0.11	0.14	0.07
MnO	0.07	0.04	0.09	0.01	trace	0.03	--	--
S	0.24	0.26	<0.1	?	0.58(SO_3)	0.04	0.37	1.1

[a] Does not include carbon

Table 3. Trace-Element Analyses of Argillaceous Rocks (ppm)

Element	Hole UE17e[26] Average (8 Sa)	Hole UE17e[26] Standard Deviation	Heater Site[27] Average (6 Sa)	Heater Site[27] Standard Deviation	Average Shale[28]	Ordinary Pierre Shale[25]
Ba			99	17	580	730
Cl	36	13	40	10	180	130
Co	36	4	29	9	19	13
Cr	154	45	112	33	90	80
Cu	24	1	20	6	45	36
Mo	8	7	2	1	3	1
Pb	23	4	15	7	20	22
V	177	42	125	28	130	170
Zn	112	28	61	20	95	130

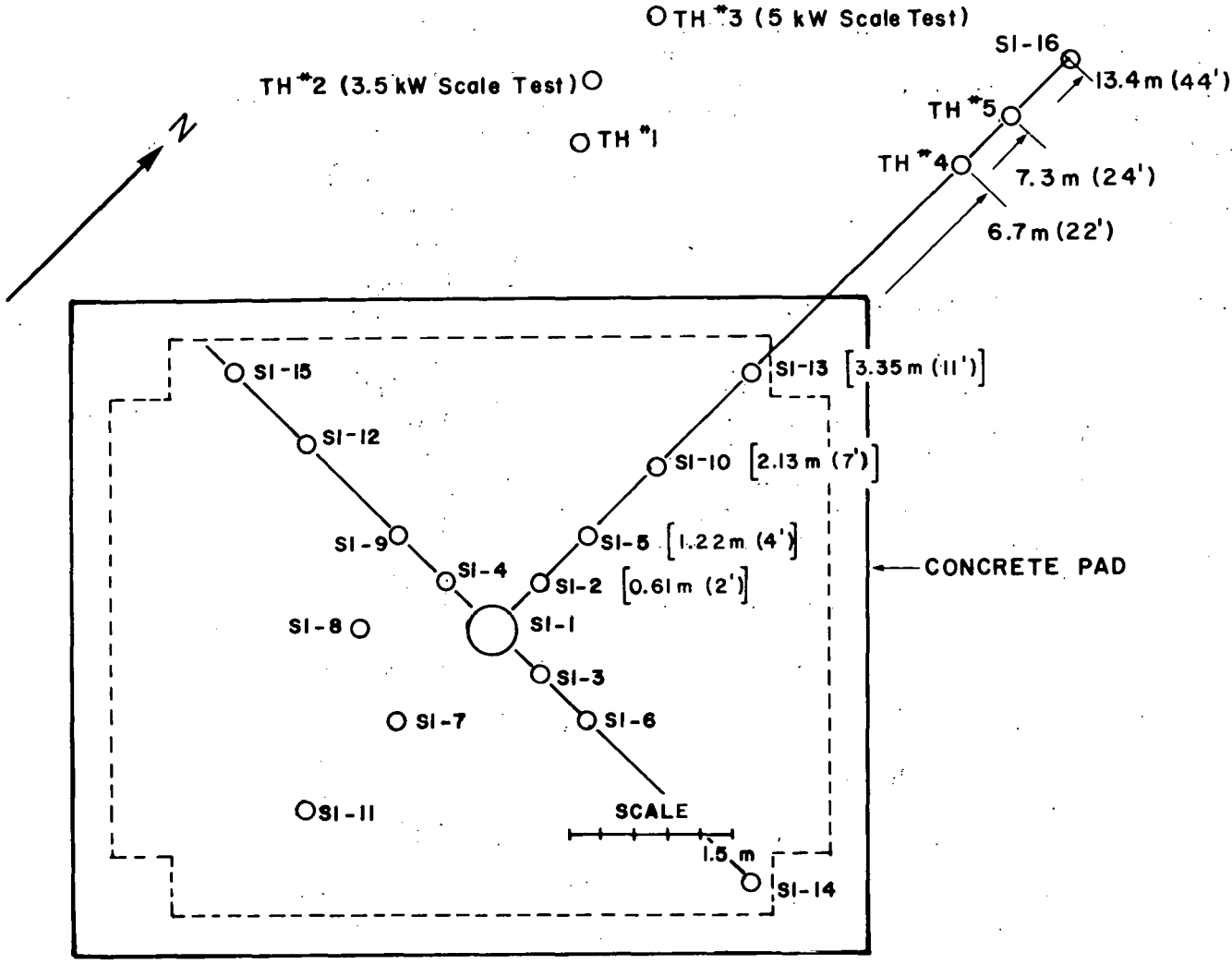

Figure 4. Plan View of the Heater Site, Eleana Near-Surface Heater Experiment

Drill holes along the radius between S1-1 and S1-13 are parallel to the strike of the argillite (N10°E) and contained the primary thermal instrumentation for the experiment. The heater was installed in S1-1. Thermocouples installed normal to strike and along the radius between S1-1 and S1-15 provided a limited measurement of anisotropic thermal behavior. Holes along the radius between S1-1 and S1-14 were used to monitor volatile pressures, while vertical rod extensometers were emplaced in Holes S1-7, S1-9, and S1-11. Hole S1-8 was used for emplacing vibrating-wire stress gauges. Table 4 specifies the detailed functions of each drill hole; Table 5 gives instrumentation details for all instrumentation except the heater.

Hole S1-1 is nominally 0.36 m in diameter. All other holes are 0.10 m in nominal diameter. The nominal depth of the holes is between 24.4 and 28 m. Exceptions were S1-1, which was extended at 0.20 m diameter to 33.5 m, and S1-3, extended at 0.10 m diameter to 35 m.

The heater used, shown schematically in Figure 5, consisted of a sealed cylinder of 304 stainless steel containing radiative heating elements. Nominal inside diameter of the cylinder was 0.30 m; the outside diameter was 0.32 m. The heating elements were tubular Chromalux units 0.013 m in diameter, each rated at 6 kW maximum power. The elements consisted of nichrome resistance wire twisted into a helical coil, embedded in MgO ceramic, and enclosed in a stainless-steel sheath. Each element was in the form of a hairpin loop ~3.7 m long. In this configuration, the heated length of each loop was 2.9 m. A heavy conductor on the last 0.75 m at each end of each

element replaced the nichrome wire; thus the electrical connections at the ends of the elements were not heated directly. The heater contained six element loops wired in two sets of three for three-phase, 240-V operation.

Table 4. Drill Hole Function Summary

Hole	Function
S1-1	Heater hole, sump for water collection, with rock-wall thermocouples at 22.9 m
S1-2	Measure temperature at 18.6, 19.2, 20.1, 21.0, 21.95, 22.9, 23.8, 24.7, 25.6, and 27.1 m
S1-3	Measure volatile pressure at 18.3 m (bottom of casing), emplace pump for water removal, monitor water temperature
S1-4	Measure temperatures at same depths as in S1-2
S1-5	Measure temperatures at 19.2, 20.1, 21.0, 21.95, 22.9, 23.8, and 24.7 m
S1-6	Measure volatile pressure at bottom of casing (18.3 m)
S1-7	Measure vertical displacement between surface and depths of 19.8, 21.3, 22.9, and 24.4 m; record temperatures at 19.8 and 24.4 m
S1-8	Measure radial, tangential, and intermediate stresses at 22.9 m
S1-9	Same as S1-7
S1-10	Measure temperatures at 19.2, 21.0, 21.95, 22.9, 23.8, and 25 m
S1-11	Same as S1-7 and S1-9
S1-12	Measure temperatures at 19.2, 21.0, 21.95, and 22.9 m
S1-13	Same as S1-10
S1-14	Same as S1-6
S1-15	Same as S1-12
S1-16	Measure background temperatures at 22.6 and 23.2 m

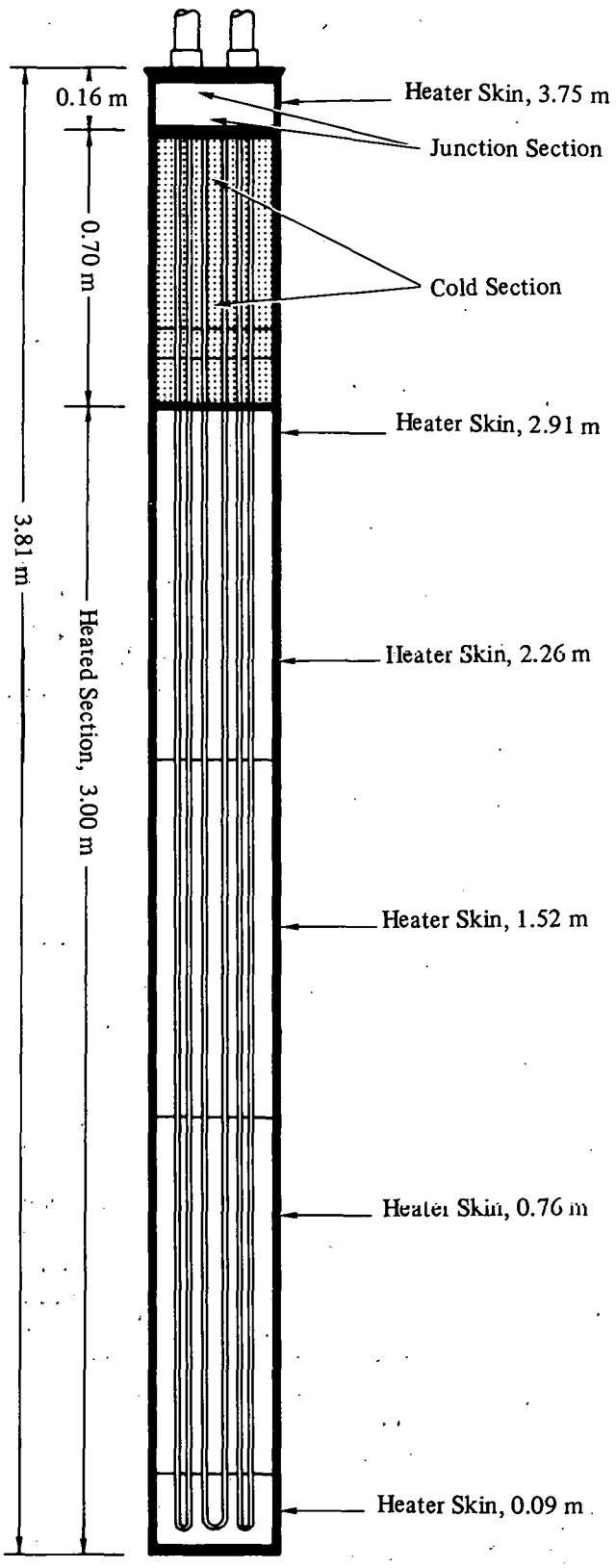

Figure 5. Schematic Cross Section of Heater (Positions of diagnostic thermocouples are also shown)

Table 5. Instrumentation Descriptions and Method of Emplacement

Measurement	Transducer Type	Description	Specific Purpose
Temperature	Thermocouples	Chromel-Constantan Type-E, in (Mg-O filled) stainless-steel sheath. TCs were strapped to rigid PVC tubing for installation and then grouted in place by injection grouting through tubing. Alignment controlled by alignment of tubing.	Thermal field measurements in formation
	Thermocouples	Same as above except clamped to internal heater parts or in single vertical channel (covered) on heater surface.	Heater diagnostics and skin temperatures
	Thermocouples	Chromel-Alumel Type K mounted on top and bottom vertical extensometer anchors.	Extensometer data correction as a function of temperature
Volatile or Gas Pressures	Gulton Type GS613 Diaphragm 0 to 100 psi range	Installed either at drill collar or at bottom of packers. Packers located just above the bottom of casing in holes designated for pressure data, and also in the heater hole.	Monitor gas pressures in the formation
Vertical Displacement	Invar Rod Extensometers	Four extensometer rods used in each hole. Each rod was stainless steel to bottom depth of casing, and then Invar to TD, where it was anchored to hole wall. The top end of each rod was attached to an LVDT, the electrical readout of which was calibrated against displacement.	Measurements of changes in vertical distances in the formation as a result of heat.
Stress	Irad-Creare vibrating-wire gauge with short-term 200°C capability.	Gauges emplaced in aluminum tubing, calibrated, and potted before installation. They were grouted in drill holes with an expandable grout, thus relieving some of the preapplied stress.	Obtain qualitative information of thermally induced horizontal stress charges
Gas Transmissivity	Geiger-Muller tubes	Kr^{85} was injected in main heater hole, or surrounding instrumentation hole. A string of four probes installed in a neighboring drill hole detected time of arrival and relative intensity of tracer gas. Experiment performed both pre- and posttest.	Obtain qualitative data on amount and location of test-induced fracturing of rock

The overall heater assembly consisted of (1) the heated region, (2) the cold section, and (3) the junction section. The region containing the heated portion of the elements was backfilled with air at ambient pressure; the cold section containing the unheated portions of the heating elements was filled with expanded vermiculite. (This high-porosity material had a low thermal conductivity and was used to limit heat losses from the end of the heater.) Electrical power connections to the heater elements were made in the junction section. Two pipes 0.05 m in diameter, extending to the surface, were connected to the junction section. One carried the power leads; the other was a conduit for diagnostic thermocouples inside and on the surface of the heater. Air was forced down the power lead conduit and back out the thermocouple conduit, cooling the junction section.

Figure 6 is a generalized schematic of the heater-emplacement geometry. The heater was initially suspended ~0.03 m above the top of sump hole, but may well have been resting on the shoulder after heating, because of stretching of the suspension cable. Emplacement in an open hole permitted removal of the heater in case of electronic failure, and also permitted posttest heater removal and examination of the heater-hole wall.

A batt of fiberglass insulation bound with string was located just above the heater. At emplacement there was a gap of 0.15 m between the bottom of the insulation and the top of the heater. The fiberglass was released to expand against the holewall by burning through the string with a heated nichrome wire after heater installation. The insulation was intended to limit not only end losses of heat from the heater, but also convective transport of heat and/or fluids above the heater. A pneumatic packer installed near the bottom of the casing isolated the uncased part of the heater hole from the surface.

The data-acquisition system used in the experiment is shown schematically in Figure 7. A John Fluke data logger was the central element. Most thermocouple data were read directly into the logger at preset intervals ranging from minutes to hours. The data logger printed out these data for all channels in sequence at each print time and entered them on magnetic tape. Vertical-displacement, pressure, and heater-diagnostic data entered a low-level scanner that fed into the data logger; the function of the low-level scanner was to increase the total number of data channels to 120. The Creare-IRAD stress-gauge data were digital and needed to be converted to analog form before printout. A microprocessor controlled a printout terminal; thus data for successive printouts of each channel appeared in sequence.

The data-acquisition system was mounted in a van and powered by a diesel generator with a backup demand-start generator. A telephone dialer system interfaced with the data logger called the operator off-hours in the event of heater malfunction. A Variac power control unit for manually controlled constant power operation of the heater was also located in the van. Data processing of the magnetic tapes was done at Sandia's Data Reduction Center in Albuquerque.

Table 6 lists the estimated precision of the various instrumentation used in the heater test. The values given, however, do not include possible field-related effects, nor temperature effects in the case of extensometer and stress data. Accuracy of the various measurements in the field is considered in Appendix A. Estimated limitations are such that all measurements, except for the temperatures within the argillite, must be regarded as qualitative.

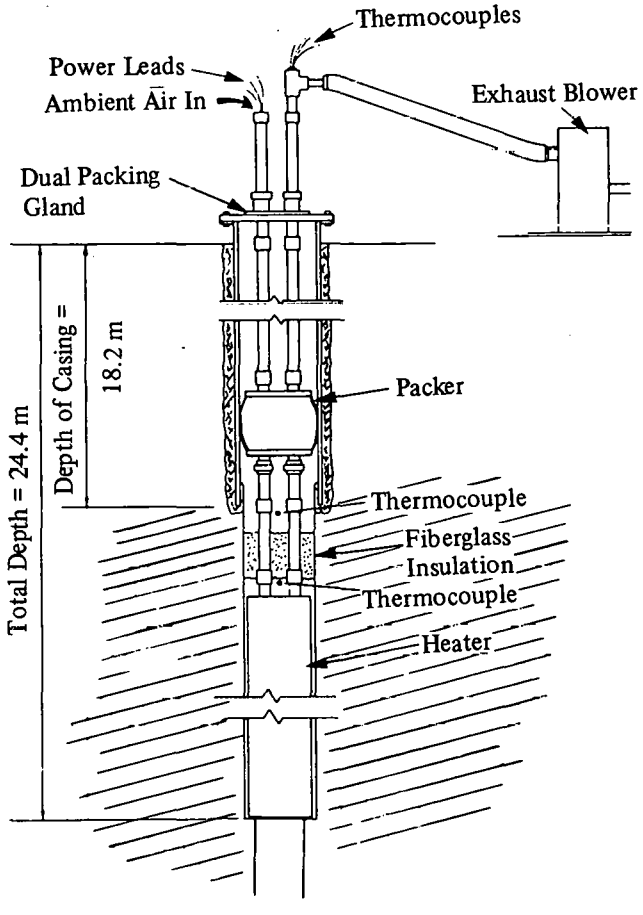

Figure 6. Schematic Cross Section of Heater-Emplacement Geometry

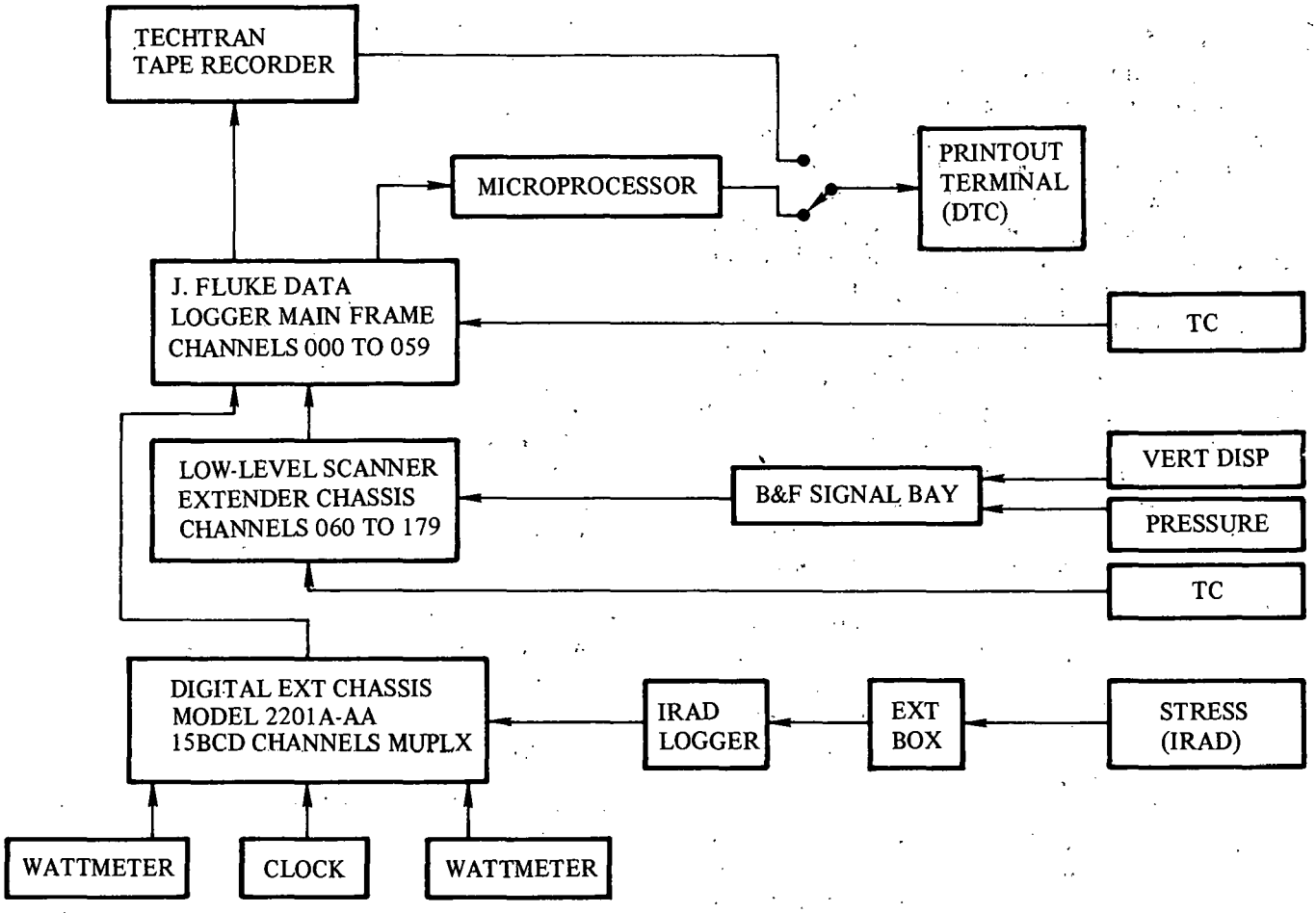

Figure 7. Data-Acquisition System

Table 6. Summary of Estimated Precision in Experimental Measurements.*

Measurement	Transducer	Experimental Error
Heater Power	Magtrol Model 4610 Digital Power Analyzer	±0.3% of reading ±0.05%
Temperature	Thermocouples	±1°C
Stress Change	Creare Vibrating Wire Cages	±15% at ambient temperature
Vertical Displacement	Potentiometer-extensometers	$\pm 13 \times 10^{-5}$ m at ambient temperature
Gas Pressure	Gulton GS613 Diaphragm Gages	±1%
Transmissivity	KR 85 Flow Intensities	±? qualitative only
Water Collection	Bucket	? apparently variable

*The experimental errors listed are estimates of precision, and do not include an estimate of emplacement-related limitations.

Modeling

It is assumed that the results of field tests can be evaluated only through description and modeling of the phenomena observed during testing. Therefore, it is necessary to describe the modeling carried out for the Eleana heater test before discussing results.

Thermal calculations were made with the finite-element code COYOTE.[32] The axisymmetric model configuration consisted of 360 quadrilateral elements, each with eight nodal points (Figure 8). The region included in the analysis was a cylinder 13.5 m in radius and 42.6 m in length, with the 0.178-m-radius heater hole in the center; outer boundaries were assumed adiabatic. Initial temperature was set at 18°C. The argillite was assumed uniform throughout the modeled volume, with the orthotropic, temperature-dependent thermal conductivities listed in Table 7. Heat capacity values used are shown in Figure 9.

Note that the data in Table 7 and Figure 9 ignore two potentially important factors. Thermal conductivity parallel to the axis of core material was measured by means of guarded-end-plate measurements. Radial measurements were made with transient-line-source techniques. The fact that layering was inclined at ~30° was ignored. In radial measurements, the data reduction scheme assumes that the material is radially symmetrical. Thus the conductivity data, while gathered in a manner consistent with the modeling approach used, involved some compromise.

Specific heat data shown in Figure 9 were modified from experimental data by removing the spike near 100°C, caused by vaporization of water remaining after pulverizing of the samples, and replacing it with the heat of vaporization of 3% by weight water. For compatibility with the computer code, vaporization was assumed to occur between 50° to 105°C. This treatment of water volatilization had two implications. First, it assumed that dewatering is not instantaneous at 100°C. This is consistent with more recent work on welded tuffs, which indicates that much of the water loss from the matrix of water-bearing rocks may occur by vapor-pressure-driven diffusion rather than by simple boiling.[33] The temperature ranges over which such a mechanism operate depend on both the local geometry and heating rates. Secondly, the heat capacity treatment used here assumed *de facto* that the water vapor was instantaneously removed from the system after generation, since no further account was kept of its behavior. This obviously makes the treatment incomplete in any portion of the model where there is appreciable fluid tranport.

Table 7. Measured and Modeled Thermal Conductivities of Eleana Argillite (W/m°C)

Measured T(°C)	A	B
25	--	2.43
50	--	2.17
75	1.74	--
100	1.73 → 1.62*	2.06
150	1.49	1.80
200	1.42	1.67
250	1.36	1.69
300	1.31	1.73
350	1.29	1.61

Modeled T(°C)	C	D
20<T≤80	2.15	2.75
80<T<150	2.15-0.0089(T-80)	2.75-0.0143(T-80)
T≥150	1.53-0.0010(T-150)	1.75

Key to Letter Coding

- A Average of two samples measured parallel to core axis
- B Average of four samples measured radial to core axis
- C Perpendicular to modeled layering
- D Parallel to modeled layering

*Decrease results from holding sample near 100°C for 24 hours

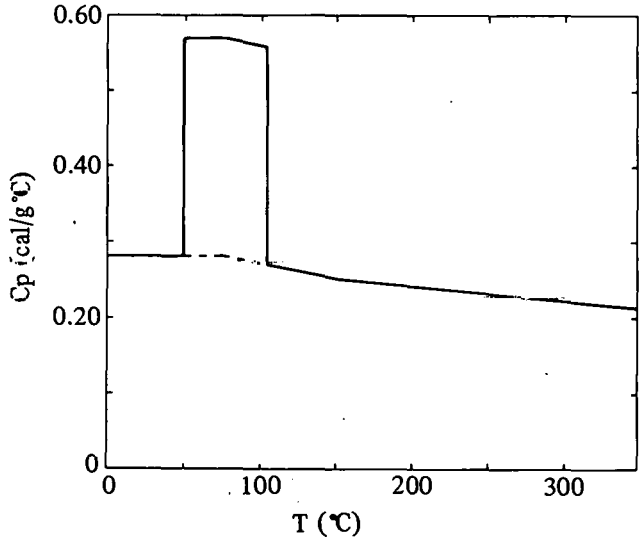

Figure 9. Heat Capacity as a Function of Temperature, as Assumed in Thermal Model

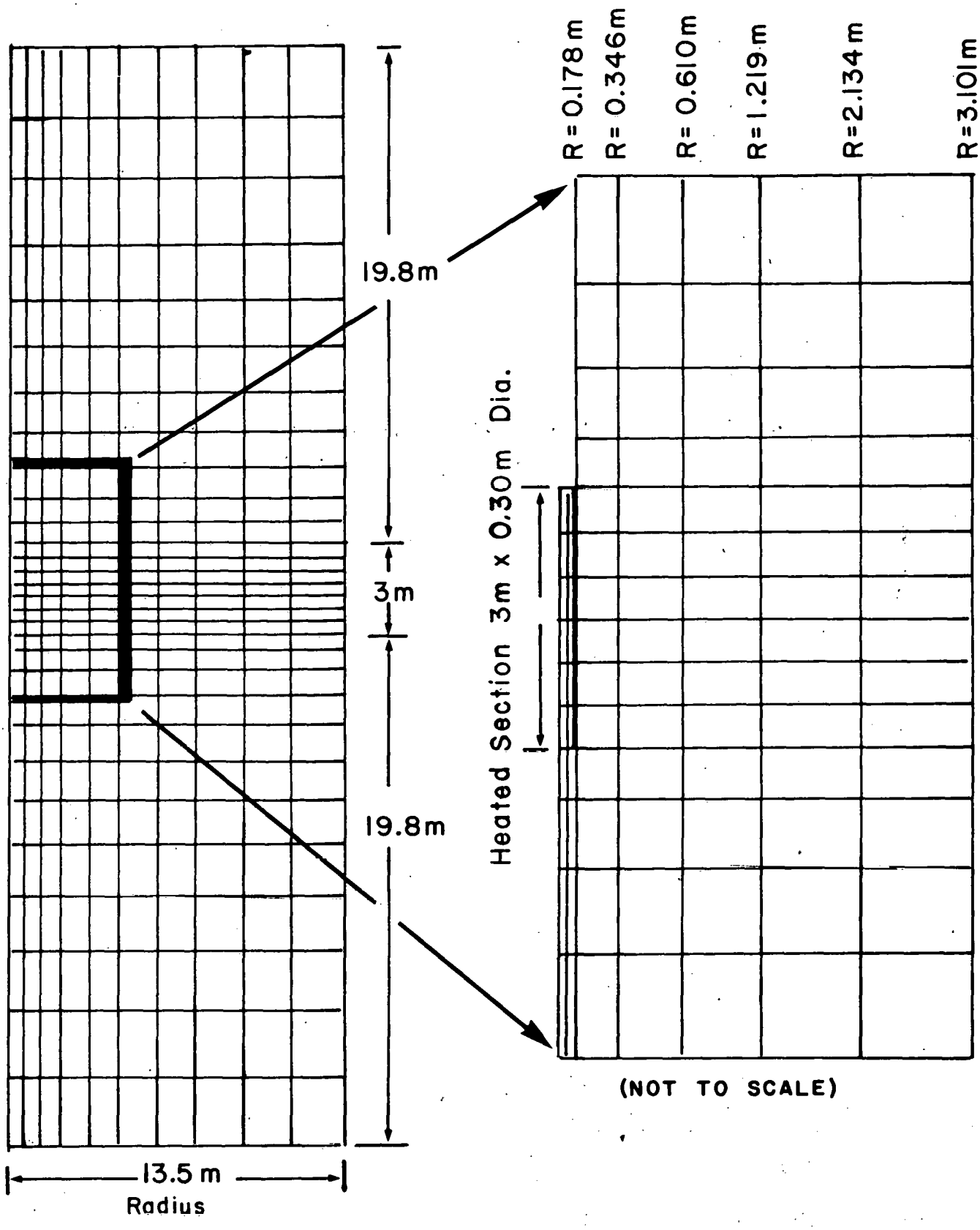

Figure 8. Finite-Element Mesh Used in Thermal Analysis

Heat transfer across the air gap between the heater and the rock was assumed to be by means of combined radiation and conduction. Vertical and radial convection was ignored in the air gap opposite the heated section of heater because the ratio between heat transferred across a gap by convection plus conduction to that transferred by conduction alone is near unity for the range of gap Rayleigh numbers in the experiment configuration.[34] In addition, the ratio of gap length to gap width was large enough to preclude significant vertical transport by convection. It was assumed that all of the power input into the heater was radiated and/or conducted radially across the gap between the heater and rock. The modeled results should, therefore, result in maximum estimated temperatures. A literature-derived temperature-dependent heater surface emissivity was also used. Details of the effective conductivity formalism are given in References 35 and 36.

In the thermal model, it was assumed that the insulation at the top of the heater was at a uniform temperature of 90°C from the beginning of the test, as was the top surface of the heater. The conductivity of the cold section of the heater was assumed to be 1 W/m°C, and conductive heat transfer from the top of the heated section to the top of the heater was allowed. The top surface of the insulation batt and the hole wall at all points above this level were assumed adiabatic. Results of thermal modeling are described at the same time as experimental results, since temperature measurements were the most abundant measurements made during the test.

An analysis of thermal stresses was made using Sandia's modification of the ADINA code.[37] This general-purpose linear and nonlinear finite-element program for static and dynamic problems contains an element library with 1-D, 2-D, and 3-D continuum elements, in addition to an extensive materials library. Transient temperature distributions calculated with the COYOTE code were input to the stress calculation. Hence, the overall geometry and dimensions of the analysis regions were the same. The mechanical model had 459 four-point quadrilateral elements, with 500 nodal points. Initial in-situ stresses were in most cases not considered in the analysis. The outer and bottom boundaries of the model were assumed fixed with regard to radial and vertical displacements, respectively. The ground surface and borehole surfaces were assumed traction-free.

As described above, the Eleana Formation is highly jointed. It is thus apparent that argillite possesses little tensile strength in-situ. In compression, however, argillite displays a nearly constant elastic modulus and finite crush strength, followed by strain softening. The assumed constitutive and failure models are shown in Figure 10. Note that temperature, confining-pressure and time-dependent effects on failure were not included in the model because of the limited data available.

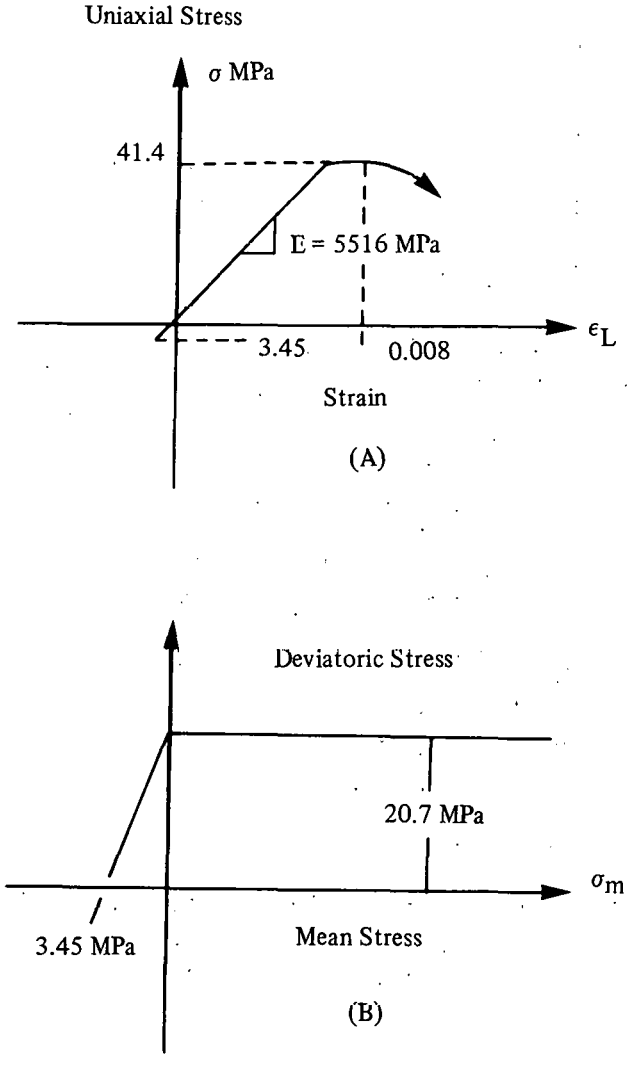

Figure 10. Assumed Constitutive (A) and Failure (B) Behavior of Eleana Argillite

Also, as previously mentioned, the argillite contains varying amounts of expandable clays. Upon heating to or near the local boiling point of water (or as a result of sufficient exposure to dry air even at ambient temperature), the expandable clays partially dehydrate and contract. Ambient pressure measurements of the linear thermal expansion of argillite have shown a linear contraction of ~1% between 75°

and 125°C, followed by a nominal expansion at higher temperatures (Figure 11).[38] Based on these data, the thermal expansion behavior shown in Figure 12 was assumed for the argillite.

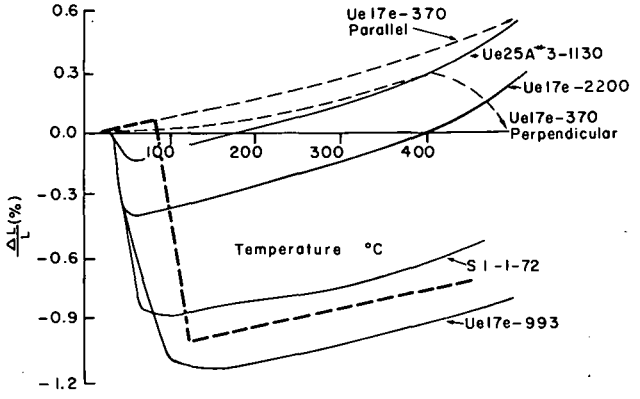

Figure 11. Ambient-Pressure Thermal Expansion Measurements on Eleana Argillite (Behavior assumed in mechanical modeling is shown by heavy dashed line)

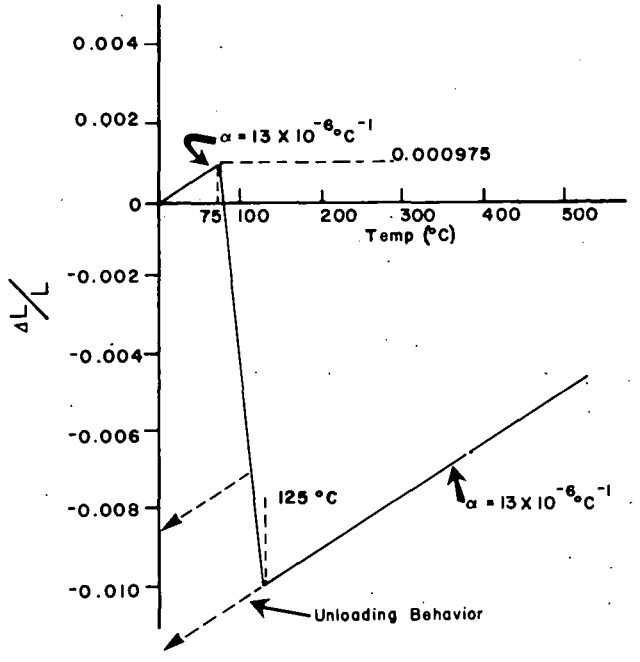

Figure 12. Details of Assumed Thermal Expansion Behavior of Eleana Argillite

It was further assumed that the thermal expansion/contraction behavior of argillite is isotropic. This restriction is not inherent in the code, but was made in the light of the paucity of available data. There is good evidence, in fact,[39] that some argillaceous rocks undergo anisotropic contraction upon dehydration. Second, it was assumed that the argillite, once dehydrated, did not rehydrate and therefore did not follow in reverse the same curve on cooling as on heating. Also note the assumption that the argillite would begin to dehydrate near 75°C regardless of the local heating rate.

Tensile failure was calculated to occur in specific stress-dependent orientations if a principal tensile stress exceeded the tensile failure stress of the argillite. In this case, it was assumed that a plane of failure developed perpendicular to the stress direction, independent of preexisting joints. The calculated effect of this failure was to reduce both the normal and shear stiffnesses across the plane of failure, and to release the corresponding normal stress. This calculational procedure markedly limited the propagation of tensile stress relative to similar calculations that did not include a tension cutoff.

In summary, the thermal and mechanical models used for modeling the Eleana Near-Surface Heater Experiment were current, but did not result from extensive code development. Anisotropic thermal properties were considered only to a limited extent. Dehydration of the rock mass was considered only by modifying the terms of the heat capacity and thermal conductivity. No consideration was given to the vaporized water because of the implicit assumption that it left the system immediately after generation.

No attempt was made to couple the mechanical calculations with potential changes in thermal properties resulting from mechanical deformation. Such coupling might prove of major importance, but its understanding awaits further code development and analysis of field data. In the approach used here, joints were predicted to form only as a result of thermal contraction and were always oriented either along conical or cylindrical sections centered on the heater or on plane surfaces parallel to the heater axis. In reality, given the inherently complex jointing of argillaceous rocks, radial anisotropy could probably be imposed on in-situ thermal response independent of bedding orientation, as a result of radially anisotropic joint distribution.[40] Because they are so strongly linked to overall interpretation of the experiment, yet could not be directly verified or contradicted by field measurements, the results of mechanical modeling studies are described below.

It was assumed that argillite began to contract at 75°C, and that calculated tensional stresses resulting from contraction were accommodated by the opening of joints within the volume of rock at temperatures $>\sim$85°C. The calculated extents of such zones at three different times in the experiment are shown in Figure 13.

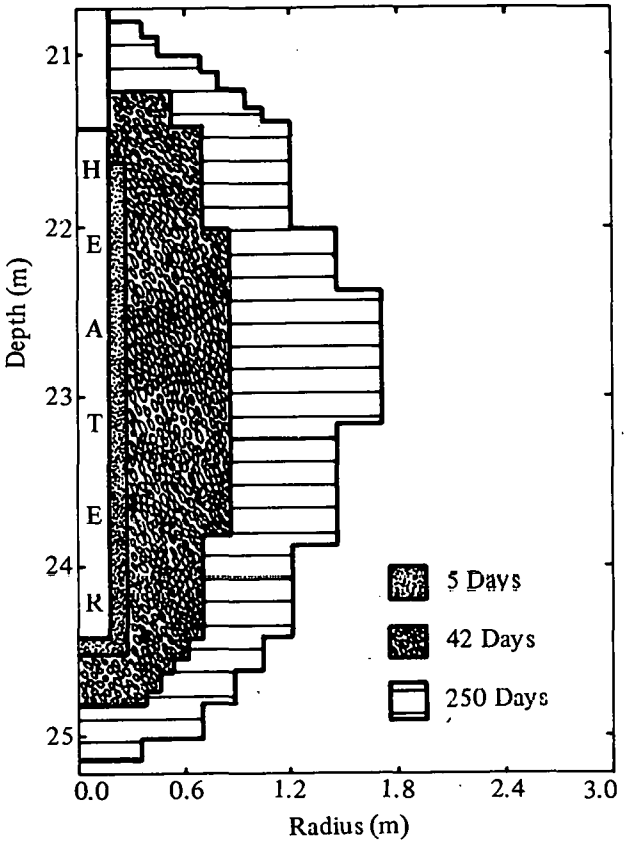

Figure 13. Calculated Zones of Tensile Fracturing at 5, 42, and 250 Days

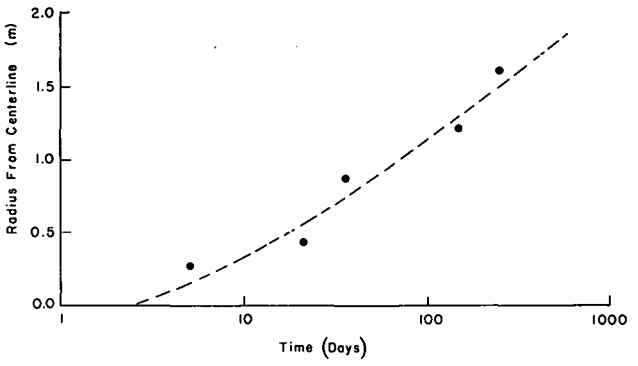

Figure 14. Calculated Radius of the Zone of Tensile Fracturing as a Function of Time

At a time of 5 days, only a very small area around and at the bottom of the heater was predicted to have contracted, and to contain newly formed tensional joints. At 42 days the radius of the zone of contraction was calculated to extend beyond the 0.61-m radius of the first instrumentation holes. At 250 days, the contracted volume extended slightly beyond the 1.22-m radius of the second set of instrumentation holes. By this time, the rock was also calculated to have fractured to a depth of ~0.7 m immediately below the heater, and for nearly as far along the hole above the heater. Figure 14 shows the calculated radial extent of the contracted zone as a function of time.

Reduction of the assumed Young's modulus of the argillite from 6896 to 2068 MPa had no discernible effect on the calculated radius of the cracked volume at a time of 150 days. Variation of the maximum linear thermal contraction between 0.2% and 2% also had little effect. The calculated radius of the cracked volume at 150 days was 1.2 m if 0.2% contraction was assumed, and 1.5 m if 2% was assumed.

One major effect of the postulated contraction of the argillite was to greatly reduce predicted compressive stresses near the emplacement hole. Figures 15 and 16 show the modeled radial and tangential stress distributions to a radius of 1 m at times of 5, 21, and 42 days, respectively. At 5 days, compressive radial stresses were at a maximum between 0.5 and 0.7-m radius opposite the center plane of the heater and decreased both away from and towards the heater. A stress concentration was also present near the base of the heater.

At 21 days, the maximum calculated compressive stress zone moved out to a radius of between 0.8 and 1+ m and interconnected with the zone at the bottom of the heater. An irregular zone of volumetric contraction was present along the hole wall, extending to a maximum radius of ~0.25 m. Stress gradients near this boundary were so sharp that the contracted-volume boundary would virtually coincide with the slightly positive isobar shown. At 42 days, apparently because of radial relief into the contracted volume around the heater hole, the 1.5-MPa isobar opposite the heater center plane disappeared, and was represented only by isolated remnants above the top of the heater and at the base. Similar results have been found in large-scale or global modeling studies in argillite.[41]

Predicted tangential stresses behaved like radial stresses in many respects, as shown in Figure 16. At 5 days, stress contours were quite smooth and the only marked concentration was in a small zone near the top of the heater. At 21 days, the 2.0-MPa contour formed a zone opposite the heater center plane with a radius of 0.4 to 0.8 m and lower stresses on both sides. At 42 days, this contour moved out to between 0.8 and 1+ m, and tangential relief of volumetric contraction occurred out to a radius of ~0.5 m. One

difference between the radial and tangential results was that tangential stress concentrations tended to occur above the top of the heater, while radial stress concentrations occured at the bottom. The results indicate that at a representative location (say at a radius of 1 m opposite the heater center plane), the radial stress maximum should have been reached before the tangential, but that neither stress should have been anywhere near the assumed compressive failure stress of 41.4 MPa.

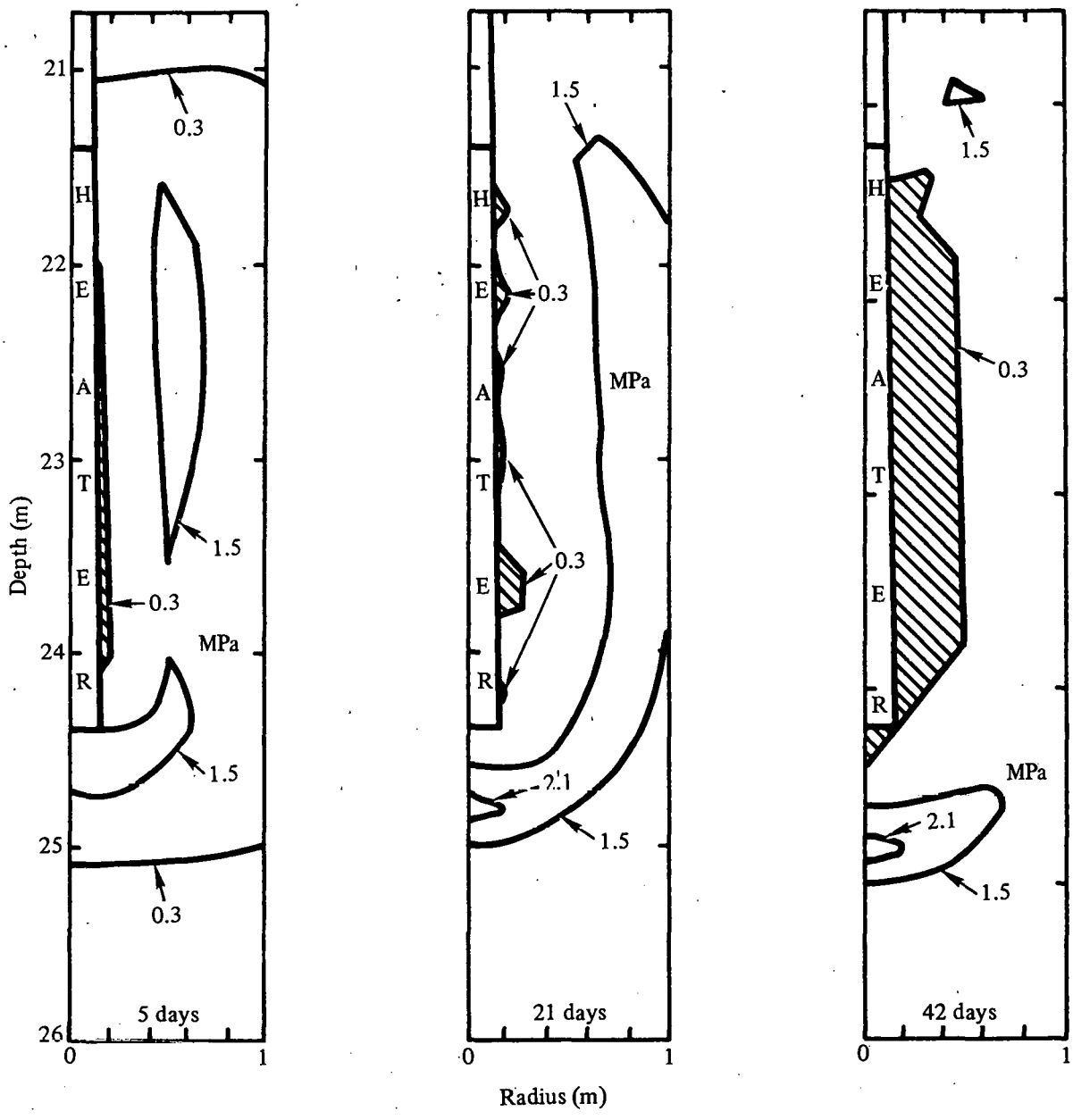

Figure 15. Calculated Radial Stress at 5, 21, and 42 Days

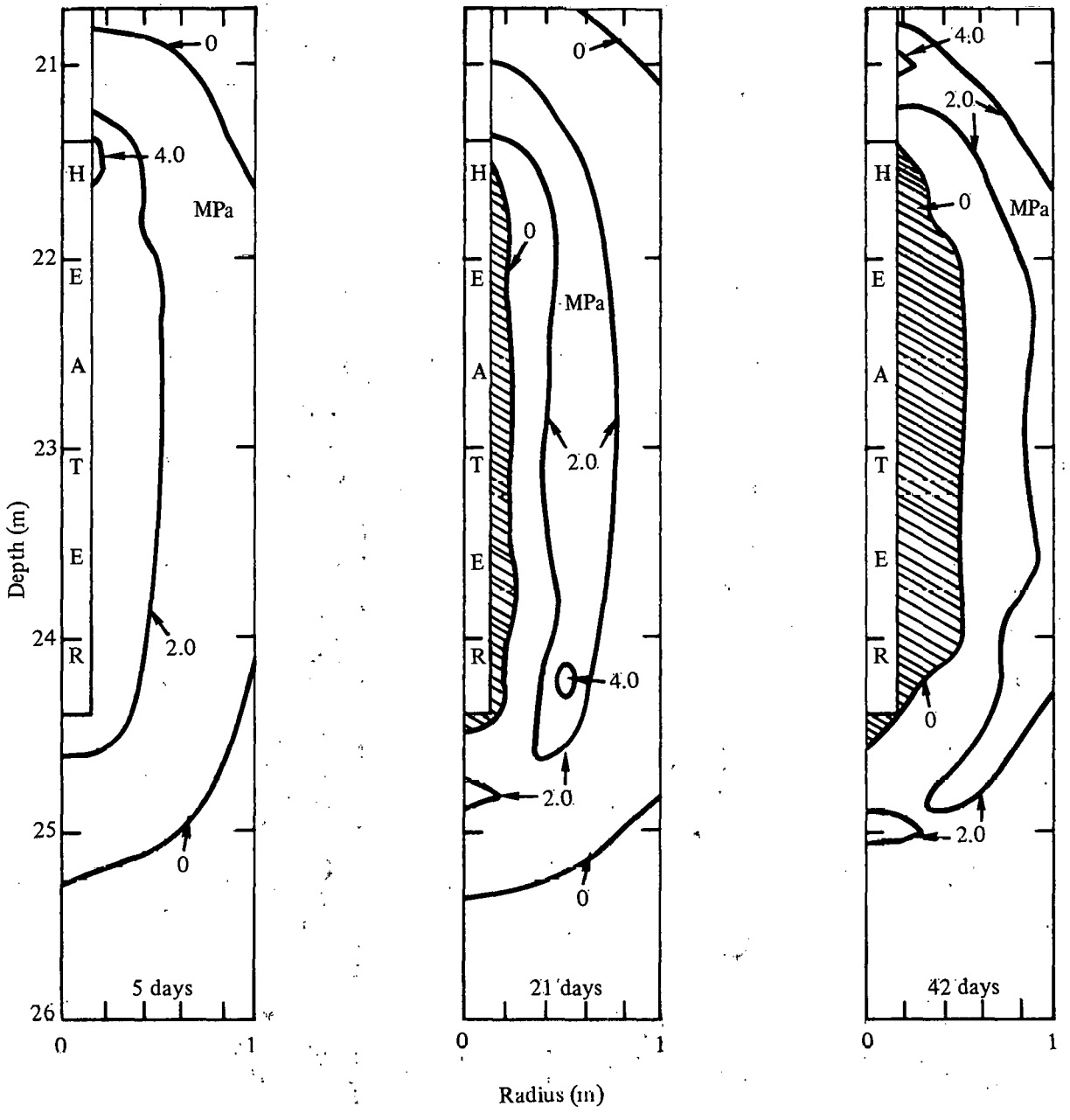

Figure 16. Calculated Tangential Stress at 5, 21, and 42 Days

Operational History, Test Results, and Comparison With Modeling

The approximate site for the heater experiment was chosen in May 1977, based on drilling results at Hole UE17g, which encountered weathered rock to a depth of only 16 m and was located next to the experiment site. The concrete pad and drill collars were emplaced in July 1977. Drilling at the experiment site was completed in February 1978.

The heater for the test was fabricated at the EG&G Atlas facility in Las Vegas, Nevada, during the first quarter of FY78, and was installed in S1-1 March 21, 1978. At this time S1-1 had a nominal depth of 24.4 m and S1-3 of 28.2 m; these holes were not connected. After final hookup, the heater was turned on at a power level varying between 2 and 2.2 kW at 1 p.m., April 4, 1978. This portion of the test was shut off at 1 p.m. on April 10 after 120 hours of operation, because of problems caused by water present in the heater hole. In-hole thermal results of the initial 120

hours of operation of the heater are shown in Figure 17.

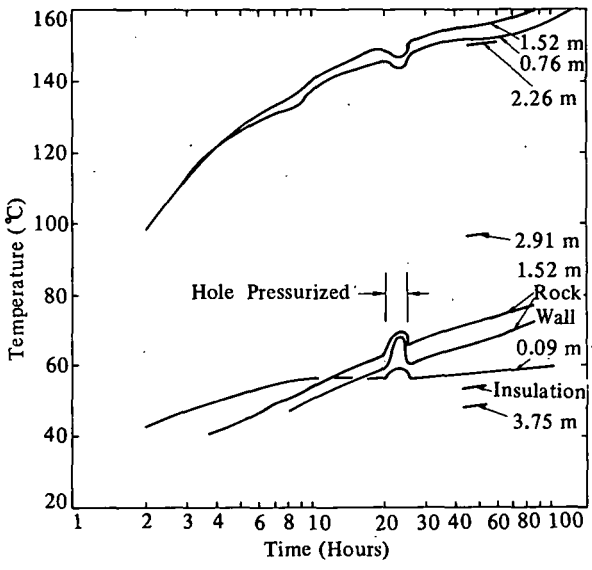

Figure 17. In-Hole Thermal Results of the First 120 Hours of Operation of the Full-Scale Heater (At the end of this time, the heater was removed. Distances are heights above the base of the heater.)

About 20 hours into the test, it became apparent that the bottom portion of the heater was covered by water. This conclusion was reached because the bottom thermocouple on the heater (at a height of 0.09 m) had reached a temperature of only ~60°C and was rapidly becoming steady-state. At the time of initial heater installation it was noticed that a very small amount of water was still present after tamping the drilling debris. This water appeared only as a few small puddles between remaining uneven areas of the hole bottom. At this stage of the test, lowering the heater onto the hole bottom apparently further compacted the drilling debris, with concomitant rise of liquid water in the annulus between the outside of the heater and the emplacement-hole wall. The water level at the beginning of the test is unknown, but must have exceeded 0.1 m. When the heater was pulled after 6 days of operation, scale deposits on the external surface indicated that the peak water height was ~0.35 m.

At 20 hours operating time, the portion of S1-1 below the packer was pressurized to 0.014 MPa for 5 hours in an attempt to drive the water from the bottom of the hole. The unsuccessful results of this effort are included in the figure. Heater-skin temperatures above 0.76 m were depressed by as much as 4°C as a result of the pressurization, while temperatures recorded by the rock-wall thermocouples at the heater center plane increased during the same time interval by as much as 8°C. The temperature recorded by the lowermost thermocouple on the heater also increased, by 4°C.

The increase in temperature near the bottom of the heater is consistent with the interpretation that the air pressure partially succeeded in removing the water from the hole, if there was a steady-state thermal gradient in the standing water in the hole. An alternative explanation is that the slight increase in gas pressure decreased water evaporation rates in the bottom of the hole by raising the boiling point, and therefore allowed a slightly higher steady-state temperature to be reached.

The opposing senses of response of the heater skin temperatures at the center plane and the rock-wall thermocouples is evidence of an increase in the effective thermal conductivity between the heater and the rock-wall. This increase could be caused by several mechanisms: induced convection from the forced flow of vapor into the formation; a decrease in absorption of radiant heat from a decrease in water vapor concentration within the gap; or a change in rock emissivity caused by a change in the rate of water evaporation. Whatever the reason, the change in effective conductivity was small.

In general, the short-term effect of standing water in S1-1 was to lower most heater temperatures slightly. The temperature at the heater center plane was 156°C after 48 hours during the first period of operation, and 174°C in the main period. This difference is very nearly the same as the relative difference in power levels of the two runs (2 to 2.2 kW versus 2.5 kW). Thus, there is little early-time effect at the center plane. Thermal gradients along the heater skin were markedly affected by the presence of the water only in areas near the standing water. At 48 hours, the difference between the temperature at 0.09 m and at 0.76 m was 93°C with the bottom of the heater submerged, versus 52°C with the bottom of the hole dry. Long-term effects of such water remain unclear.

The heater was removed from S1-1 on April 18, 1978, and deepening of S1-1 and S1-3 begun. Deepening and cross-connecting these holes required about 1 month. Cross-connection between the holes was established by use of a side-cutting water jet operating at nozzle pressures of ~100 MPa.

The heater was reinstalled in S1-1 on May 9, 1978. Instrumentation was checked, a short period of background data obtained, and the heater turned on at 2.5 kW at 1 p.m., May 16, 1978. Power was increased to 3.8 kW at 1 p.m., June 6, 1978, and held at this level until the experiment was shut off January 22, 1979. The heater was removed from the emplacement hole

March 6, 1979, and dismantling of the experiment begun. After gas transmissivity testing, the experimental site was decommissioned April 19, 1979, except for posttest coring completed in May.

Measured and modeled in-hole temperatures (except for sidewall thermocouples) during the main portion of the experiment are compared in Figure 18. Modeled temperatures at the center plane of the heater reached a peak value of 311°C, compared to a measured value of 350°C, a 11% difference relative to the experimental value. Up to ~30 days into the test, modeled and measured temperatures agreed to within 10°C or less. After this time, the two values increasingly diverged, possibly because the surface emissivity of the heater did not increase as fast upon heating as assumed.

Modeled temperatures were asymmetric about the heater center plane, presumably because perfect thermal contact between the heater and the argillite in the bottom of the hole was assumed in the model and resulted in some drawdown of temperatures on the lower half of the heater. This asymmetry was most marked by calculated temperatures at the bottom and top corners of the heated zone: the peak calculated temperature at the bottom corner of the heater was 259°C while that of the top of the heated zone was 296°C, or only 15°C below the temperature at the centerline. Measured temperatures at 0.76 m height, except during the last 90 days of the experiment, exceeded those at the centerline, at times by nearly 20°C. This sense of difference is contrary to modeled results.

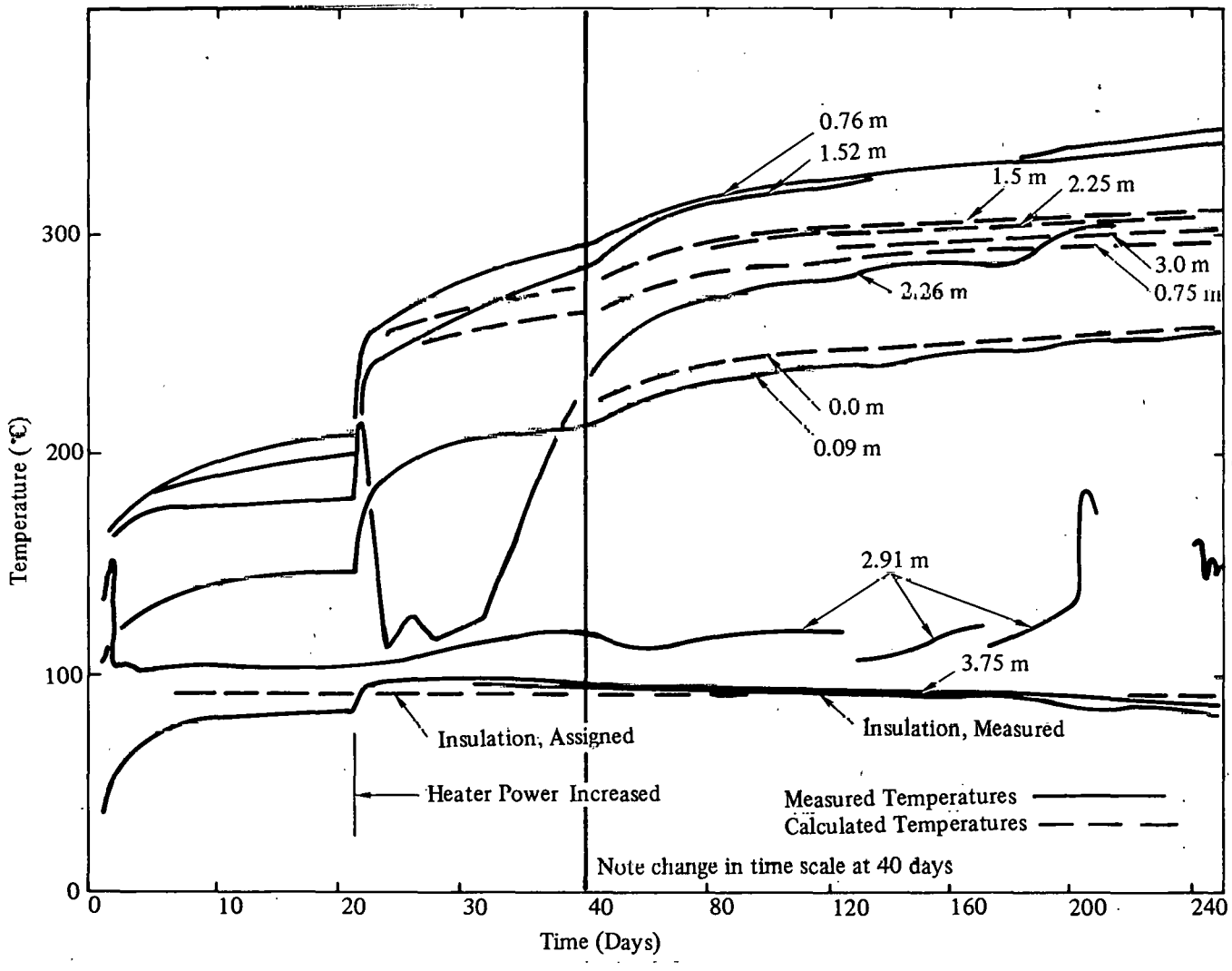

Figure 18. In-Hole Thermal Results of the Full-Scale Heater Test, Except Side-Wall Thermocouples (Heights are given in distances above the bottom of the heater)

Measured temperatures at 2.26 m were erratic. At early times they lagged behind expected results. Shortly after the power was increased, the temperature at this height was effectively limited to only slightly above 100°C. After about 60 days into the test, temperatures at this height paralleled expected values of 290° to 300°C, and appear to have reached calculated temperatures by the end of the test.

Intermittent inflow of water between 21 and about 30 days into the test may have been responsible for the anomalously low temperatures measured at this height. Examination of the heater after it was removed from the emplacement hole revealed a slight scale deposit between the surface of the thermocouple shield and the body of the heater, that extended from 2.1 to 3 m, but not to the top of the heater. That temperatures were never decreased to the local boiling point of water (94°C) probably means the water was able to affect this sheathed thermocouple only indirectly. Intermittent inflow of water, such as that proposed here, was also apparently responsible for intermittent damping of temperatures measured during one of the scaled heater tests made before the full-scale experiment.[40]

The difference between measured and modeled heater temperatures was most striking at 0.09 and 2.9-m heights. Measured temperatures at 0.09 m (253°C maximum) lagged only slightly behind modeled temperatures (259°C maximum). Measured temperatures at 2.91 m, however, lagged more than 100°C behind those expected for the entire test. Again, this appears to have been caused by periodic inflow of water. At late stages in the test, measured temperatures at 2.9 m became even more erratic, although they generally increased, as in the case of the measurements at 2.26 m.

The thermal history of the insulation was complex. At early times, temperatures of both the top of the heater and the insulation increased regularly. Shortly after the increase in heater power, both thermocouples in this area reached temperatures near 100°C, but never went any higher. Between about 25 and 40 days, both temperatures appeared to exceed the local boiling point of water.

After peaking at 30 days, temperatures at both the top of the heater and the bottom of the insulation decreased very slowly for the rest of the test. After ~40 days, the temperature at the insulation was below 94°C, eventually reaching a value of only 85°C. This cooling trend is consistent with the interpretation that input air served as a continuous heat sink in cooling the insulation. If so, then the cooling trend would indicate a continuously decreasing rate of water precipitation and condensation in the insulation after ~40 days.

Calculated and measured temperatures on the hole wall and in the rock, both at the elevation of the heater center plane, are compared in Figure 19. Measurements at radii 2.13 and 3.35 m indicated very little thermal anisotropy caused by layering, and agreed with calculated results to within 5°C or better for the duration of the experiment. Temperatures were slightly higher parallel to strike than perpendicular to it. Temperatures measured parallel to strike at 1.22 m agreed quite well with the modeled results, but were slightly higher; there were no temperature measurements at 1.22 m perpendicular to strike.

At 0.61-m radius, thermal anisotropy was increasingly evident, especially at temperatures > ~100°C. Above ~120°C, measured temperatures both parallel and perpendicular to strike exceeded modeled temperatures, indicating that in-situ thermal conductivity at these temperatures was less than that used as input for the modeling. Temperatures at this radius were also greater parallel to strike than perpendicular to strike, implying that thermal conductivity was higher at some inclination to the layering than parallel to it, in contrast to the model input data. At the end of the test, there was a difference of 30% between measured and calculated temperatures parallel to strike at 0.61 m.

Temperature measurements at the hole wall displayed a variable relationship to modeled, and were consistently more erratic than measurements in grouted holes. Measured temperatures responded more rapidly than modeled temperatures to heater turnon. Between ~6 and 40 days, modeled temperatures exceeded measured temperatures by as much as 30°C. When the power was increased at 21 days, modeled temperatures increased more rapidly than those measured. In addition, as indicated in the figure, the response of one rock-wall thermocouple was irregular for ~10 days after the increase in power level.

The lagging of measured temperatures of side-wall thermocouples behind modeled temperatures during most of the first 40 days of the test was attributable to at least two causes. It may be that the near-field effective conductivity was greater than estimated. Comparison of measured and modeled temperatures at a radius of 0.61 m indicates that this was not the case, however. It may be that the side-wall thermocouples were somehow cooled by convection or transport of water vapor that was in the emplacement hole. This is consistent with the response of side-wall temperatures to hole pressurization, and with the fact that measured temperatures

first begin to lag behind those predicted at 80° to 90°C. If such a cooling process was active, then cooling was apparently relatively constant up to ~40 days before decreasing. This response is also consistent with the decrease in water precipitation and condensation rate inferred from the temperatures of the heater insulation at times later than about 40 days.

At times > ~40 days, measured temperatures at the hole wall consistently exceeded calculated values. The difference was ~20° between 40 and 170 days, consistent with the sense and estimated magnitude of error resulting from incomplete shielding of the thermocouple, conduction down the mounting spring, and/or contact resistance between thermocouple and rock. At ~170 days there was a qualitative change in slope of the hole-wall data and an increase in difference between measured and modeled temperatures to a maximum of >40°C.

There are at least two explanations for this behavior. First, contact resistance between the rock wall and the thermocouples may have increased. It appears unlikely, however, that a marked decrease in contact would take place at the same time at two separate thermocouples separated by ~0.3 m. Secondly, in-situ thermal conductivity may have decreased in the region monitored by the two thermocouples. This is the most likely explanation, especially since the measured and modeled temperatures at a radius of 0.61 m also increasingly diverge at about the same time. The decrease in in-situ thermal conductivity is also consistent with the predicted propagation of the zone of tensile fracturing.

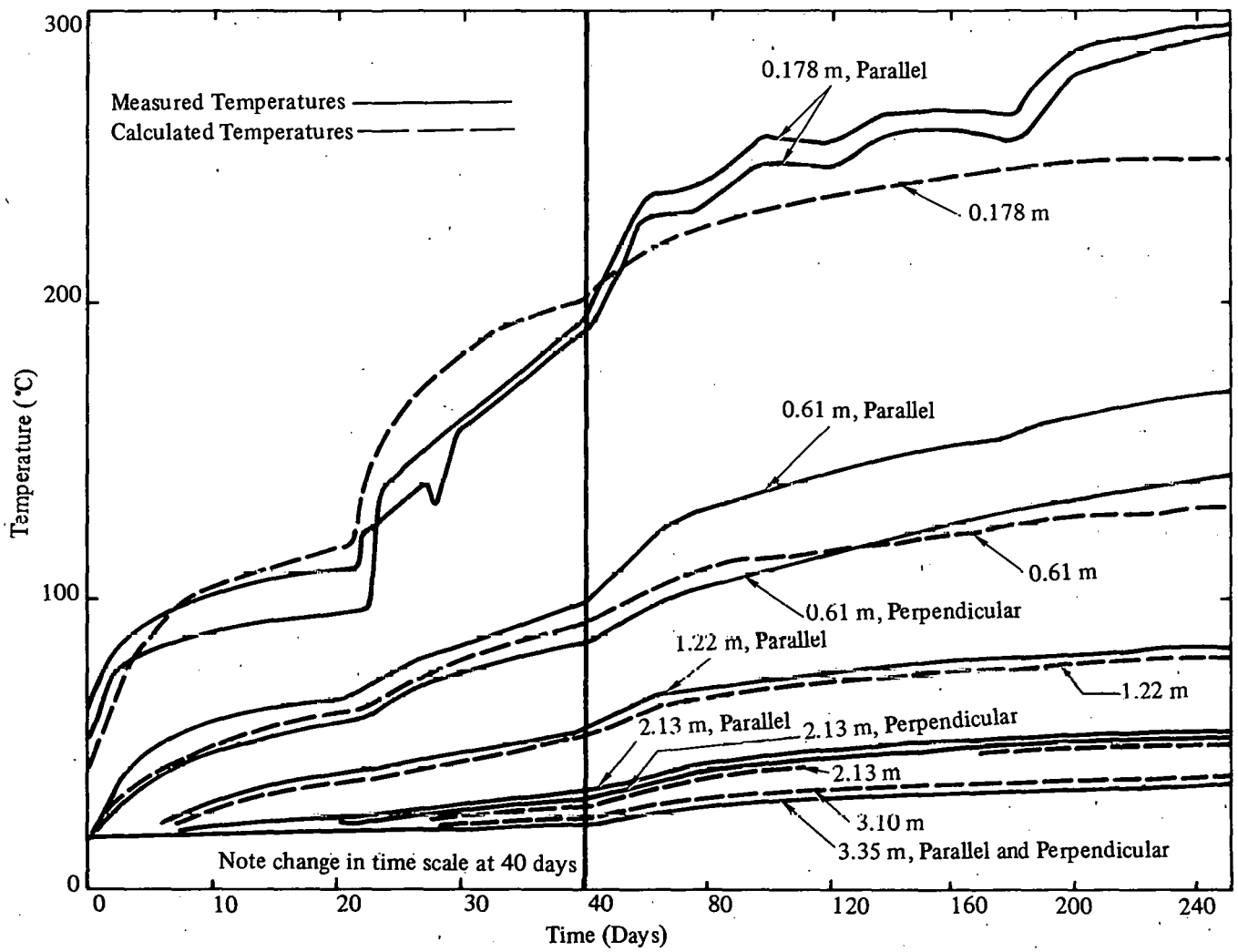

Figure 19. Argillite Temperatures at the Heater Center Plane as a Function of Time (Temperatures at 0.178 m are for sidewall thermocouples, measured parallel to strike)

Measured and modeled temperature profiles parallel to strike at two different times are compared in Figures 20 and 21. At 21 days into the experiment, there was good agreement on and near the elevation of the heater center plane. Above this level, and especially above a depth of 21 m, measured isotherms were consistently displaced upwards relative to modeled. The results appear to indicate that at least some upwards transport of heat was not fully accounted for in the modeling. For heater experiments in the Conasauga Shale, the displacement of isotherms showed that some continuous convection was taking place during this experiment,[8] since measured isotherms both above and below the centerplane of the heater were consistently displaced upwards. As shown in Figure 20, however, measured isotherms below the heater center plane here lay either on or outside the calculated isotherms, except in a small region very near the bottom of the heater. In light of this distribution, it appears that any water or steam responsible for the upward displacement of isotherms above the heater must not have formed a convective cell, but instead originated within the heated zone itself.

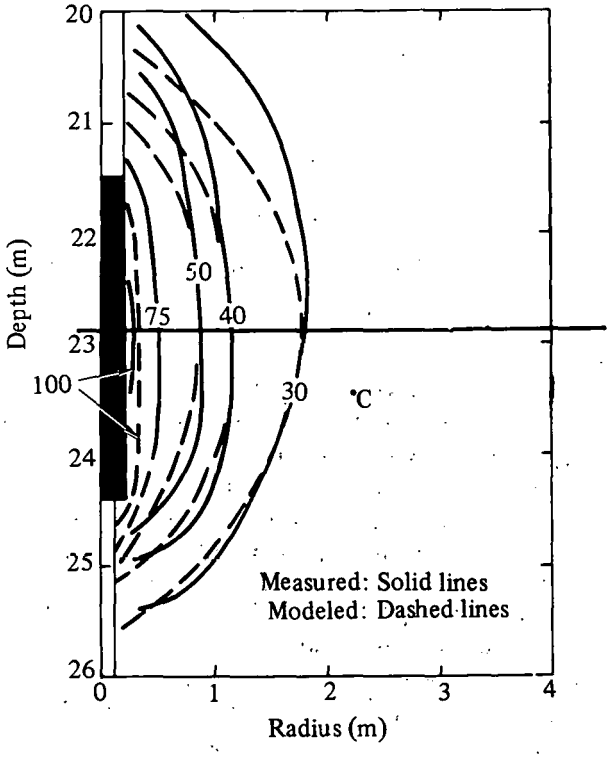

Figure 20. Comparison of Modeled and Measured Temperatures Parallel to Strike, 21 Days Into the Experiment

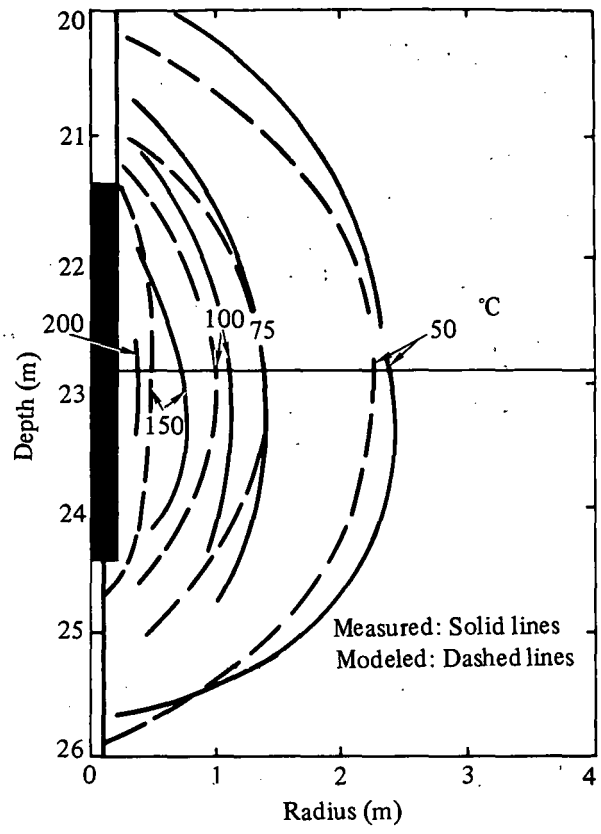

Figure 21. Comparison of Modeled and Measured Temperatures Parallel to Strike, 230 Days Into the Experiment

The situation was different at 230 days, as shown in Figure 21. The 50° and 75°C isotherms still agreed well at the heater center plane. Above the center plane, measured temperatures still exceeded modeled temperatures. However, measured temperatures on the center plane also markedly exceeded those modeled at higher temperatures. Also, while the sense of offset of the measured 100°C isotherm was consistent with earlier results, that of the 150°C isotherm is not. In the case of this isotherm only, modeled rock-mass temperatures near the top of the heater exceeded measured values. Below the center plane of the heater, as in the 21-day case, measured temperatures slightly exceeded modeled temperatures, except directly below the heater.

Contours of measured temperatures parallel and perpendicular to strike at 230 days are compared in Figure 22; definition of contours perpendicular to strike is hampered because no temperatures were measured in this orientation at a radius of 1.22 m. At a given point on the center plane, temperatures parallel to strike consistently exceeded those perpendicular to strike. This is also generally true both above and below the center plane.

In summary, there is general agreement between measured and modeled temperatures in the heater experiment. This is especially true near the heater center plane and below ~100°C. Rock-mass temperatures measured at a given radius parallel to strike consistently exceeded those measured at an analogous position perpendicular to strike. In most cases, temperatures on either side of the center plane exceeded modeled temperatures more than do those near the center plane. Comparison of measured temperatures parallel and perpendicular to strike at 230 days indicated generally higher conductivity perpendicular to strike. One consistent feature of the results was that, while modeled and measured temperatures generally agree well below ~100°C, the two temperatures increasingly diverge above this temperature.

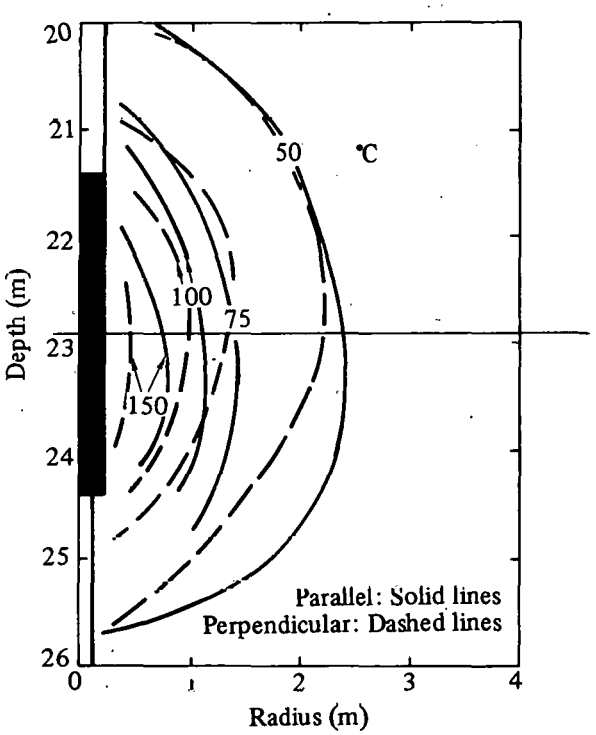

Figure 22. Comparison of Measured Temperatures Parallel and Perpendicular to Strike, 230 Days Into the Experiment

The stress response in Hole S1-8 is shown in Figure 23 and compared with modeled results. Measured data are represented both directly as stresses and indirectly as relative deformations of an originally cylindrical hole. As indicated, measurements were made in three horizontal directions: 0°, in the plane containing both the stress hole and the heater hole; 45°, at a 45° angle to this plane; and 90°, perpendicular to the plane. The measurements in the 0° and 90° orientations thus attempted to track the response of the radial and tangential stresses, respectively, about the heater.

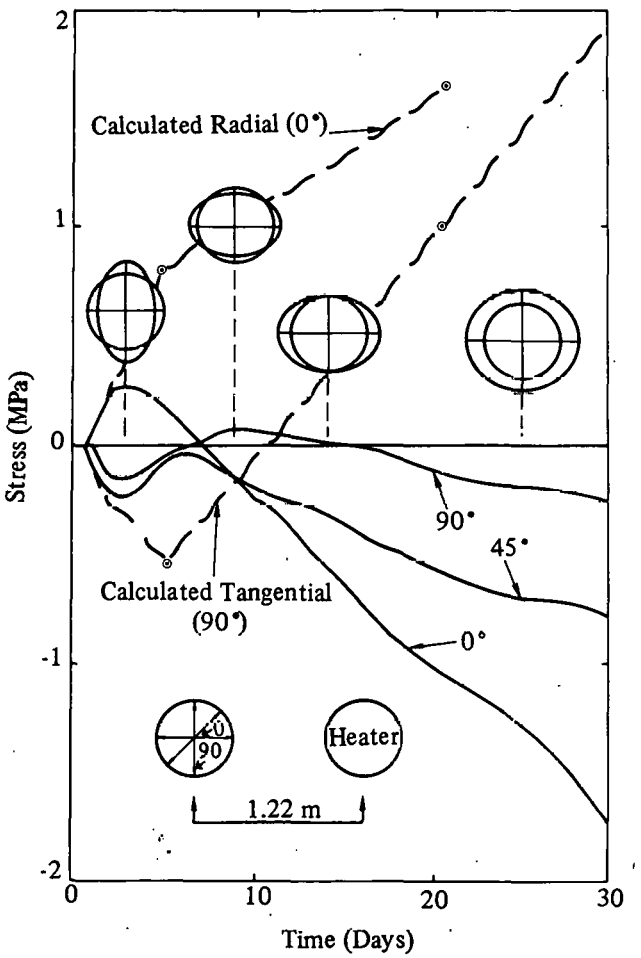

Figure 23. Stresses Measured at 0, 45, and 90 Degrees to the Line Between S1-8 and the Heater, at the Center Plane (Calculated stresses are also shown at 5 and 21 days)

For the first 3 days of the experiment, the amount of radial compression increased. Measured peak compressive radial stress was ~0.25 MPa. At this time, measurements in both the 45° and 90° orientations indicated expansion and relative tensional stresses of the same order of magnitude as the radial compression. Eight days into the test the radial stresses became tensional, and the circumferential stress became the only compressional stress. The maximum measured compressive circumferential stress was ~0.1 MPa. After 14 days, the hole containing the stress meters appeared to expand in all directions, with greatest expansion in the 0° orientation, in a plane pointing towards the heater. At 14 days into

the test, the peak temperature measured at the 1.22-m radius was 36°C, at 22.9 m depth in S1-5.

Calculated stresses at 5 and 21 days are included in Figure 23. Initial response of the measurements was consistent with modeled results, indicating compression in the radial direction and expansion in the tangential. Within ~3 days, however, measured stresses began to be much smaller than calculated stresses. Measured radial and tangential stresses of +0.25 and -0.20 MPa at 3 days compare with calculated stresses of +0.8 and -0.5 MPa at 5 days.

Both measured and calculated stresses changed ~10 days into the experiment, when tangential stress became compressive. However, the measured data indicate that only the tangential stress was positive during this period, while the modeled results indicate that both radial and tangential stresses should have been positive.

The emplaced stress-meter assemblage thus provided useful qualitative data only for ~3 days. After this time, while the change in the sign of tangential stresses was picked up, the constantly compressive radial stresses were fully relieved. It is not clear whether the long-term behavior of the stress assembly was caused by expansion of the meter and aluminum tube into the grout surrounding them, or to temperature instability of the gauge itself.

Modeled and measured vertical displacements relative to the extensometer anchor at 24.4 m are compared in Figure 24. Modeled displacements, shown by the dashed lines, were determined by subtracting the calculated displacements at 24.4 m from those at higher levels. As shown, the calculated uplift of the anchors at levels of 22.9, 21.3, and 19.8 m increases with increasing height above the reference level, with 0.76 mm the maximum uplift, for the anchor at 19.8 m. One interesting aspect of this result is that the total behavior of material at a radius of 1.22 m was expansive even though this radius is near the margin of the zone that has experienced calculated volumetric contraction by the end of the test.

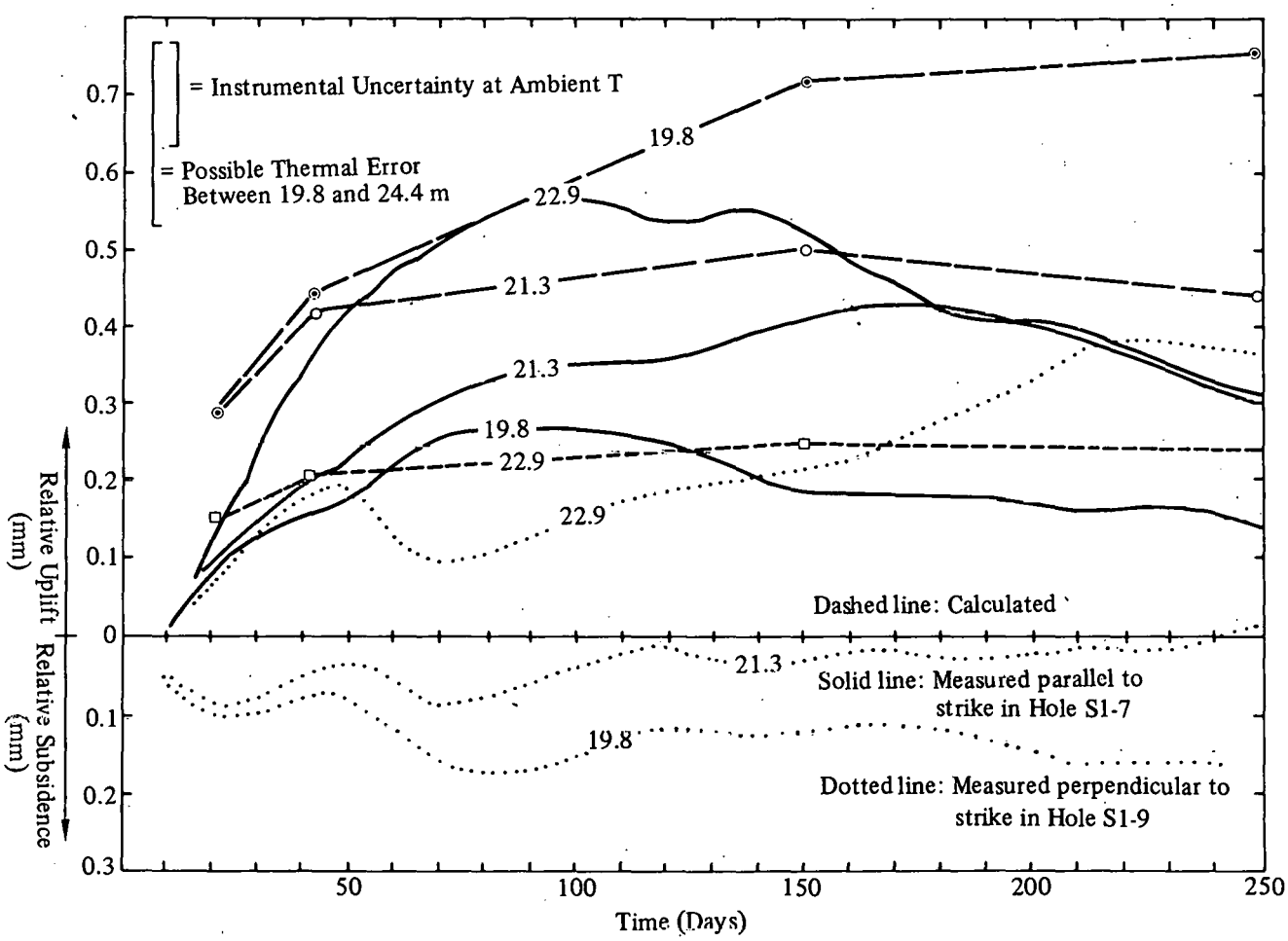

Figure 24. Relative Displacements of Vertical Extensometers, Measured Relative to the Anchor at a Depth of 24.4 m

Experimental results in Hole S1-7 parallel to strike, shown by solid lines, agreed with the calculated results in that all anchors above the reference level appear to move upwards. However, the amount of measured uplift *decreased* rather than increased with greater distance above the reference. Note that the approach of the contracted zone was apparently reflected in decreasing relative uplifts towards the end of the experiment.

Results were more complicated perpendicular to strike, as measured in S1-9 and shown by dotted lines in the figure. In this case only the anchor at 22.9 m appeared to move up relative to the reference depth, while those at 21.3 and 19.8 m appeared to subside. As in the case parallel to layering, the anchor at 22.9 m moved the most in relation to the reference level.

The potential effects of thermal uncertainties on the data shown here would be to decrease apparent uplifts with respect to the reference level. Effects would be greatest for the shallowest anchor (that at 19.8 m) both because the longest length of rod must be compensated for, and because measured temperatures were highest at the level. It is possible, if instrumental and thermal uncertainties are combined properly, to make the experimental data parallel to strike appear qualitatively consistent with modeled results. Unfortunately, potential measurement errors are of the same order of magnitude as apparent displacements. It is virtually impossible to make measured results perpendicular to strike qualitatively consistent with modeled results. Given these results, we conclude that the vertical-displacement measurements in this experiment neither confirmed nor contradicted modeled displacements.

In selecting the gas-pressure instrumentation for this experiment, we aimed to assess whether gas/steam pressures sufficient to result in volatile-induced fracturing of the argillite might be generated during the test. Consideration was not given to the fact that the maximum volatile pressures generated in any hole would be limited by the coolest portion of hole wall exposed. Thus, instead of approaching pressures required for volatile fracturing of the formation, the measured pressures shown in Figure 25 rarely exceeded 1 psig (0.007 MPa). Nonetheless, the results do indicate a local increase in permeability of the formation with time.

Removal of the cover on Hole S1-3 to allow periodic pumping of water always led to an immediate drop in the pressure below the packer in S1-1, because the holes were interconnected. In fact, in light of this interconnection, it is surprising that volatile pressures in S1-1 do not show the diurnal variations of those in S1-3.

Before 37 days into the test, gas pressures in Hole S1-6 were independent of the state of S1-3. After this time, however, the pressures in S1-6 immediately responded to the uncapping of S1-3. This indicates that communication between S1-3 and S1-6 was established between 35 and 37 days into the test. This communication need not mean that the formation was newly fractured by compression between the holes as a result of the test, but merely that enough additional joint opening occurred to allow full interconnection of preexisting fractures in the region.

Apparent water-generation rates for the first 54 days of the experiment, based on water levels in Hole S1-3, are shown in Figure 26. As indicated, the average apparent rate was $\sim 1.4 \times 10^{-4} m^3/h$, and was effectively constant for the entire period during which the experiment was collecting water. Because of the crude nature of the water-collection system, however, there is one major exception. As shown by the circled data in the figure, apparent water generation rates were almost always higher than average immediately after a pump time when the pumpdown started at a water level ≥ 2.0 m. This correlation suggests that the rock was serving as a local reservoir, and that the leaking of contained water back into the sump hole was time-dependent.

On the 52nd day of the test, the water level actually declined overnight. The experiment never again collected water in S1-3. Between days 52 and 59, the water level was relatively stable between 1.6 and 1.8 m. On day 59 this level lowered to 1.4 m; the next day and, for the rest of the test the hole was completely dry. These data help support the interpretation of increasing hole-hole interconnection near Holes S1-3 and S1-6.

Results of both pretest and posttest gas transmissivity testing are included in Table 8. Note that the numbers shown, based on either the porous-medium approximation or the assumption that the two holes are connected by a single planar joint, are qualitative.

Pretest argillite permeability, both before and after sumps were drilled in S1-1 and S1-3, was in the millidarcy range. The average value was 5.6 mD, based on 10 measurements. Posttest measurements within a radius of 1.22 m indicate an average permeability of 2.6 D, three orders of magnitude greater than at pretest. Most of the increase in permeability was local; i.e., caused by heating and not by simple drying out of the entire experimental area. This is indicated because measurements of holes outside the 1.22-m radius show a much smaller increase—from the millidarcy to 10-mD range. The dramatic increase in permeability inside a volume roughly corresponding to the modeled radius of volumetric contraction,

shown in Figure 14, shows that the modeled thermo-mechanical response of argillite is realistic.

Two inclined drill holes were drilled to the center-plane depth of the experiment after removal of instrumentation. These holes were inclined at 70° to the horizontal and were drilled as nearly parallel and perpendicular to strike as possible. The depth at which the holes should have intersected the center plane of the heater was 24.3 m. In one hole, the core recovered was completely rubbled between 23.8 and 25.9 m. This hole apparently did not intersect the heater hole, since there was no loss of core. Core from the other hole was completely rubbled from 22.8 to 25.9 m, with total loss of core recovery in the interval 23.6 to 24.4 m, indicating that the heater hole was intersected.

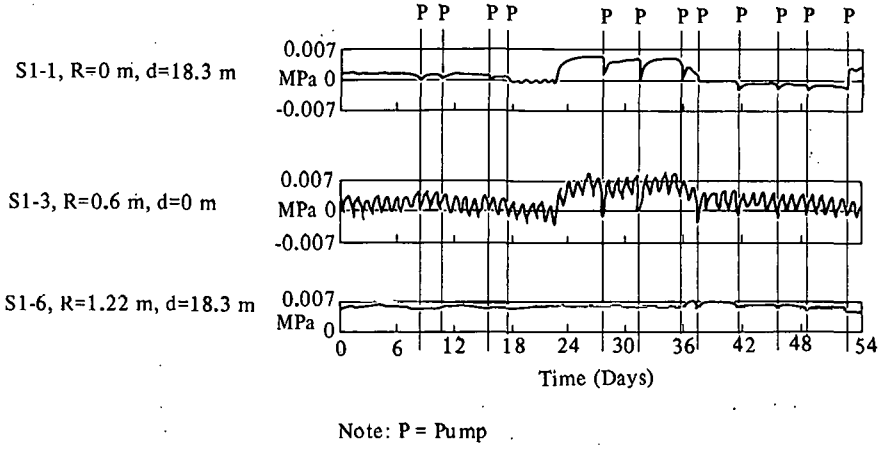

Figure 25. Volatile-Pressure Data for Holes S1-1, S1-3, and S1-6
(Vertical lines marked "P" are pump times taken from the experimental logs)

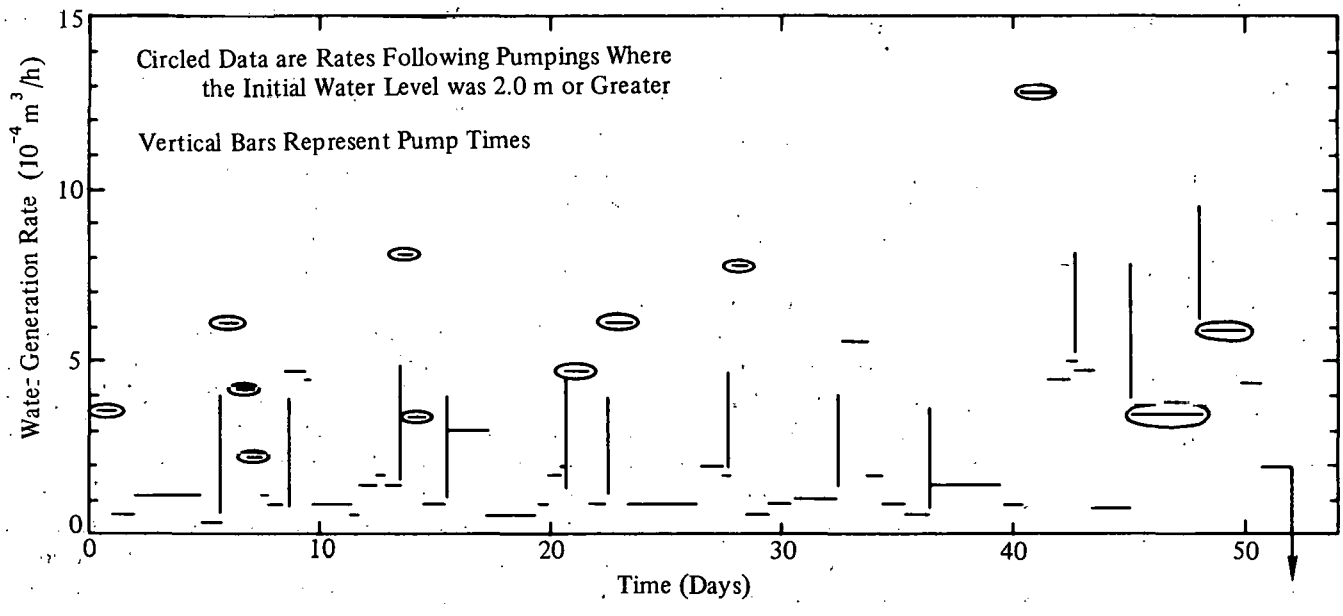

Figure 26. Apparent Water-Generation Rates as a Function of Time

Table 8. Pre- and Posttest Gas Transmissivity Meaurements of Eleana Heater Site

	K(10^{-9}ft/s)		k(Darcy)		R_H(m)
1. Before deepening of S1-1 and S1-3	Pre	Post	Pre	Post	Post
S1-1 → S1-3	3.0	4540	0.002	2.6	9×10^{-4}
S1-6 → S1-1	5.7	4640	0.003	2.7	1.75×10^{-3}
S1-6 → S1-3	14.9	4970	0.009	2.9	3×10^{-3}
S1-9 → S1-1	2.3	3680	0.001	2.1	7×10^{-4}
S1-6 → S1-14	13.5	52.8	0.008	0.03	17×10^{-4}
S1-11 → S1-1	1.9	250	0.001	0.14	4×10^{-4}
2. After deepening of S1-1 and S1-3					
S1-3 → S1-1	8.3	4500	0.005	2.6	9×10^{-4}
S1-14 → S1-1	13.8	41.1	0.008	0.024	4×10^{-5}

K = hydraulic conductivity
k = permeability
R_H = hydraulic radius

Observation of the core recovered from the posttest holes indicates only minimal macroscopic alteration. In the rubbled zone, the argillite is a dark greenish black rather than the uniform grayish black of pretest material. Limited mineralogical investigation of material from the near-heater zone indicates some alteration of the layer silicates, as shown by the results in Figures 27 and 28. In Figure 27, X-ray results are presented for a sample from a depth of 23.1 m in the drill-backhole that did not intersect the heater hole. This is above the depth of the beginning of rubble. As shown, the basal spacing of the illite decreased from 10.5 to 9.82 Å on glycolation, and increased to 9.93 Å on heating at 350°C for 24 hours. Kaolinite is almost completely stable during this treatment, and the illite peak increases in height markedly upon heating.

Figure 28 presents results for a sample from the rubbled portion of the hole that did intersect the heater hole. Here the basal spacings of the illite and kaolinite are virtually identical to those in the shallower one, but the response of both illite and kaolinite to heating is qualitatively different. In this sample, the illite peak increases only slightly in height after heating, while the kaolinite peak is greatly reduced. This indicates that the stability of both phases, but especially that of kaolinite, has been affected by the experiment. It is not clear whether the apparent degradation of the kaolinite is caused simply by an extended time (say 150 days) at elevated temperatures, or to chemical interactions in the rock. Certainly, its degradation is consistent with the reported disappearance of this phase in metamorphic sequences at temperatures ranging from 70° to 375°C.[42] That mineralogical changes were noticed here only in the layer silicate phases may well be because the major phases susceptible to nearsurface oxidation, such as siderite and pyrite, had already been removed by near-surface weathering. Chemical analyses of posttest material included in Table 9 do not indicate any significant oxidation resulting from the test when compared to at-depth or near-surface analyses included in Table 3.

The metal coupons attached to the bottom of the heater showed little reaction (Table 10). Because of the removal of water from the bottom of the hole, only those materials that could undergo oxidation in hot, relatively dry air showed any significant reaction.[44]

One final qualitative technique—borehole investigation with a cable-mounted camera—indicated some volumetric contraction from heating the argillite. As shown in Figure 29, there was considerable opening of pre-existing joints or formation of new tensional joints as a result of heating. Such joints were much less obvious and almost entirely closed in pretest observations. This phenomenon appeared to take place in Holes S1-1 and S1-3, both well within the 100°C isotherm, but was not obvious in Hole S1-6, near the margin of the modeled zone of volumetric contraction.

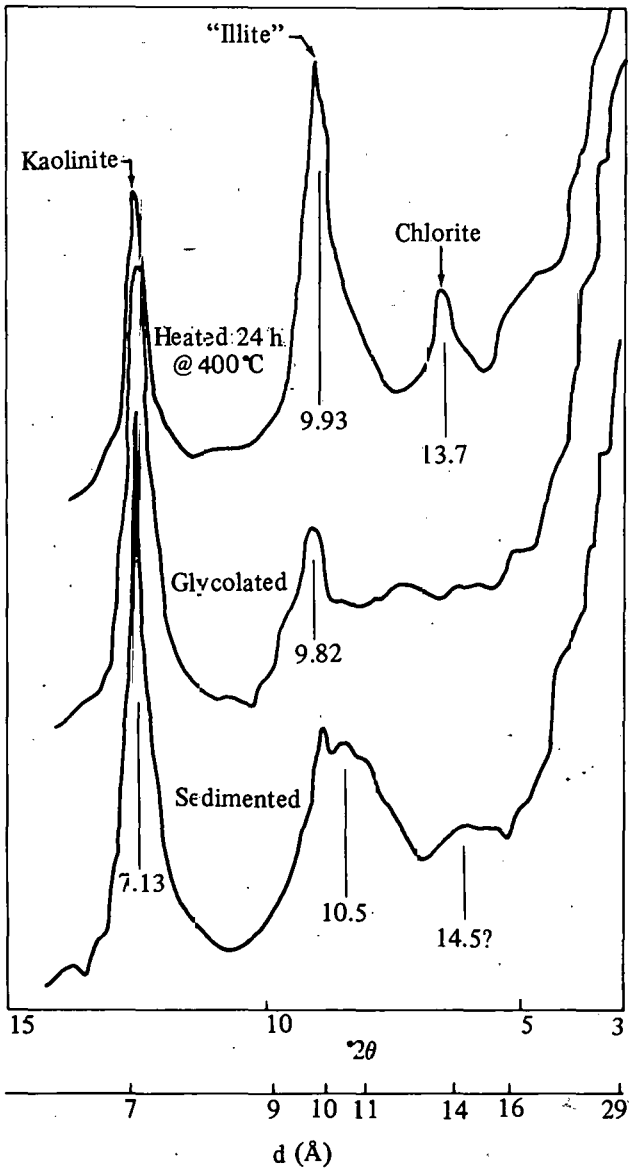

Figure 27. X-Ray Powder Diffraction Results, Posttest Sample S1a-75.7 (The curve is normalized to the quartz peak at 4.26 Å)

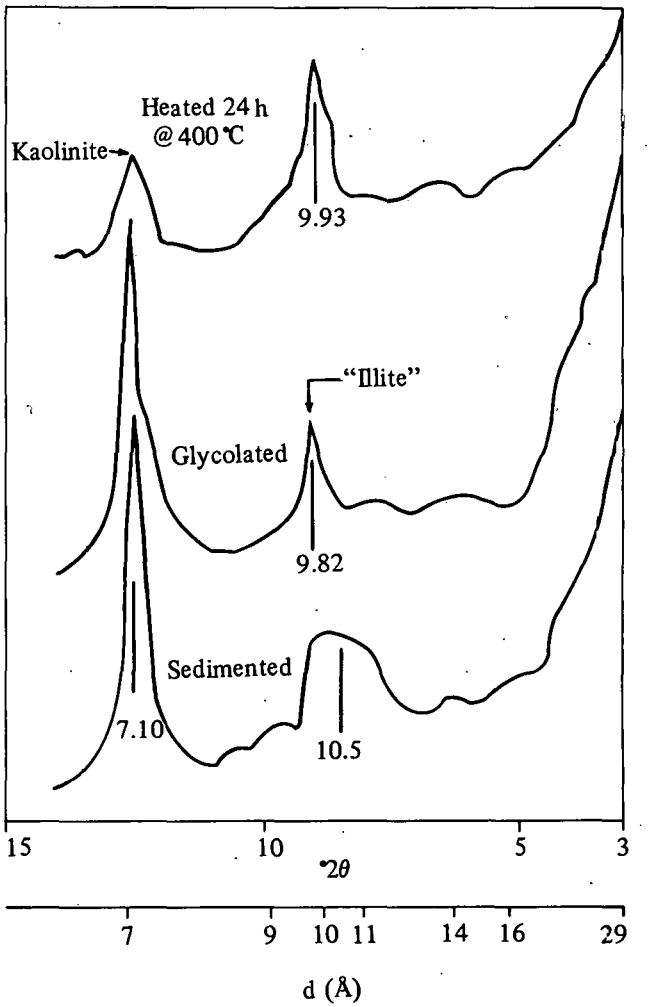

Figure 28. X-Ray Powder Diffraction Results, Posttest Sample S1b-77.8-78.0 (The curve is normalized to the quartz peak at 4.26 Å)

Table 9. Posttest Bulk Chemical Analyses, Eleana Argillite[43]

Oxide	Hole 1 23.4-23.5 m (Solid)	Hole 1 24.8-24.9 m (Rubble)	Hole 1 25.9-26.0 m (Rubble)	Hole 2 23.3-23.5 m (Rubble)	Hole 2 23.7-23.8 m (Rubble)	Average of Analyses 2-5	1σ
SiO_2	60.3	58.2	54.6	59.6	60.6	58.2	2.6
Al_2O_3	18.9	19.5	22.0	17.9	17.3	19.2	2.1
Fe_2O_3	0.45	0.72	0.22	0.70	0.69	0.58	0.24
Fe_2O	3.50	3.92	5.18	4.77	4.85	4.68	0.54
MgO	1.20	1.23	1.40	1.35	1.29	1.32	0.07
CaO	0.70	0.71	0.79	0.74	0.75	0.75	0.03
Na_2O	0.40	0.43	0.38	0.23	0.37	0.35	0.09
K_2O	1.44	1.47	1.58	1.35	1.23	1.41	0.15
MgO+CaO +K_2O+Na_2O	3.74	3.84	4.15	3.67	3.64	3.83	0.23
H_2O+CO_2(tot)	11.18	11.70	12.14	11.56	10.97	11.59	0.48
TiO_2	0.96	0.98	0.97	0.94	0.94	0.96	0.02
P_2O_5	0.2	0.20	0.21	0.20	0.20	0.20	0.0
MnO	0.07	0.09	0.11	0.11	0.12	0.11	0.01
S	<0.1	<0.1	<0.1	<0.1	<0.1	<0.1	--

Table 10. Compatibility Results of Corrosion Coupons Exposed During the Eleana Heater Experiment

Alloy	Reduction in thickness (mm)*	Remarks
1018 Steel	0.0206	Significant oxidation
4130 Steel	0.0083	Superficial surface pitting
Aluminum	0.0002	Significant oxidation
SS-316L	nil	Tarnish
SS-20Cb3	nil	Very slight tarnish
SS-Nitronic 50	nil	Very slight tarnish
SS-Ebrite 26-1	nil	Tarnish
Incoloy 825	nil	Very slight tarnish (~30 A)
Inconel 600	nil	Very slight tarnish (~30 A)
Monel 400	0.0005	Thick tarnish
Ticode 12	nil	Slight tarnish
Zircaloy 4	nil	Gold tarnish

*Note: "nil" corresponds to <0.0001 mm reduction in thickness

Heavy line: Joint large enough to have apparent depth in scan

Light line: Minor joint, apparent only as trend in scan

Figure 29. Posttest Condition of Heater-Hole Wall at a Depth of 23.5 m (Figure is drawn from borehole televiewer scan)

Conclusions and Discussion

Two main conclusions are reached as a result of the Eleana Near-Surface Heater Experiment:

1. Based on the general agreement between modeled and measured temperatures and on the lack of any compressive failure of the heater-hole wall, there is no *a-priori* reason that argillaceous rocks are not attractive for purposes of nuclear-waste management.
2. Based on the increasing divergence of modeled and measured temperatures at high temperatures and the apparent coupling of thermal and mechanical properties in-situ, additional testing would be required to characterize adequately the in-situ response of argillaceous rocks to the emplacement of heat-producing wastes. This is especially true if those rocks contain appreciable expandable clays, and if temperatures resulting from waste emplacement lead to any large amount of rock-mass dehydration.

Note that the first conclusion necessarily includes some limitations. The experiment described here was near-surface. As a result, initial in-situ stresses were negligible, and the entire experiment took place well above the water table. Creep of the argillite, which could be a major factor at depth, was not a factor because of the absence of in-situ stresses. The potential for compressive stresses around the emplacement hole was also minimized. That the entire experiment took place well above the water table means that rock-mass dehydration occurred at very near ambient pressures, and that refluxing of water was transient.

Observations also indicate that the response of Eleana argillite to heating involves volumetric contraction of the rock at the test depth, accommodated by either opening of preexisting joints or creation of new fractures. This conclusion is based on the following:

1. While measured and modeled temperatures in the argillite below ~100°C agreed well, there was increasing difference between the two values at higher temperatures. This behavior indicates a process was operative by means of which in-situ thermal conductivity at higher temperatures decreased more than simple matrix conductivity.
2. Posttest gas transmissivity testing indicated that formation permeability within a radius of ~1.2 m increased by roughly three orders of magnitude as a result of the test. This radius coincided approximately with the 85°C isotherm.
3. Pre- and posttest observation of the heater-hole wall indicated that many joints opened up during the course of the experiment. This phenomenon was also evident at 0.6 m radius, but not at 1.2 m.
4. The observations above are consistent with mechanical modeling based on the argillite thermal expansion behavior observed in the lab, in which argillite undergoes ~1% contraction between temperatures of ~75° and 125°C.

The results of this experiment contrast in part with results of the Conasauga Near-Surface Heater Tests operated below the water table, in which in-situ thermal conductivity did not decrease markedly with increasing temperature, and in-situ permeability near the heater holes decreased during the course of the test.[8]

If time-dependent effects are ignored, the extent of volumetric contraction on rock-mass dehydration and the relationship between rock-mass properties and in-situ stress should control the presence or absence of zones of absolute contraction resulting from in-situ heating. Compilation of several mechanical-modeling results for the experiment described here allows the one-dimensional approximation of this relation (Figure 30) to be made. In Figure 30 the estimated linear tensile stress ($E\Delta L/L$) at the time of maximum thermal contraction is compared with the overburden or in-situ stress, assuming a rock density of 2.6 Mg/m^3. If peak tensile stress exceeds in-situ stress by more than the assumed tensile strength of the rock, joints open; if not, they do not. The stronger a rock mass is, the greater the depth to which tensional joints would remain open at constant percent contraction. Temperature-dependent softening of a rock mass, and especially creep, would tend to offset or limit the opening of tensional joints at depth. In the case of the Conasauga tests, the in-situ rock-mass modulus may have been so low that the rock mass collapsed around the contracted zone, even at near-surface stress levels.

As pointed out above, one apparent result of in-situ volumetric contraction aside from a possible collapse is a marked increase in formation permeability. This was observed in the Eleana test, but not in the Conasauga experiments. In addition to the possibility of general formation collapse, mineralogical reactions in the Conasauga tests may have precipitated new phases in existing joints and reduced permeability. Although not obvious in limited posttest observations within the rock mass,[8] precipitation of gypsum and anhydrite definitely occurred in the heater hole during this test.

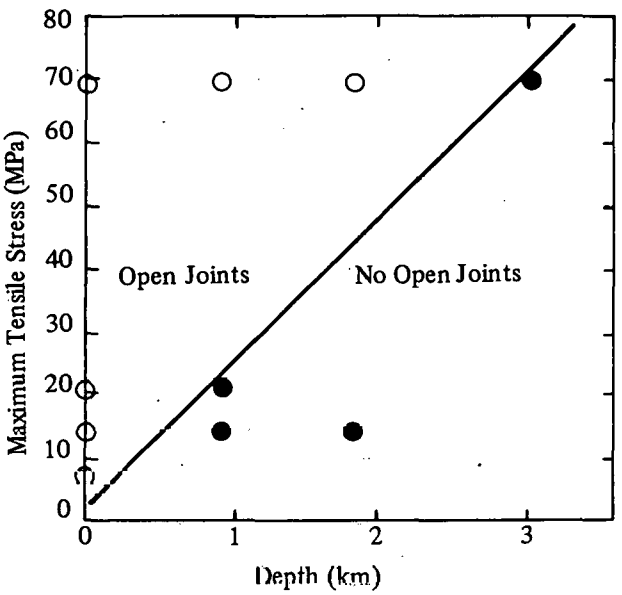

Figure 30. Calculated Depth-Joint Opening Relationship for Argillaceous Rocks

Additional complexities affect extrapolation of experimental results across the water table. In the present study, it was necessary to assume a constant temperature at which argillite began to contract on heating. In real application, this temperature would be controlled below the water table by the interaction of in-situ mechanical stresses, permeability, fluid pressures, and heating rates. This potential coupling cannot be adequately modeled at present, nor are the required data available.

Concerning the coupling of in-situ thermal contraction and conductivity, it was originally assumed that any near-hole failure would probably result from compressive failure. If so, the time scale over which failure would occur would be brief and the response of heater/canister temperatures rapid. In the actual test, however, dehydration of the entire volume within a radius of ~1.22 m resulted in a gradual decrease in average thermal conductivity, and in a gradually increasing divergence of measured and modeled temperatures. In retrospect this behavior indicates that instrumentation should have been placed in the rock at radii that were uniform rather than exponentially increasing away from the hole wall. Only in this way could the marginal degradation of an entire volume of rock be adequately documented.

Although fluid flow was not directly measured in the area of the heater during the test, experimental results indicate additional contrasts to emplacement of heat sources in the response of argillaceous rocks below and above the water table. In the Eleana test, the displacement between measured and modeled isotherms appears to indicate that only fluid evaporated out of the heated volume of rocks was active in heat transfer, and that the effect of this water decreased as the radius of the contracted volume increased. The limited recycling of water did not result in any appreciable mineralogical reactions, except for apparent degradation of some layer silicates. In the case of the Conasauga tests, refluxing of water was apparently continuous, resulting in the precipitation of a shale-anhydrite boot around the base of one heater. The overall mineralogical response of argillaceous rocks to waste emplacement might thus be much simpler above than below the water table.

The Eleana Near-Surface Heater Experiment did not qualify either argillaceous rocks as a whole or argillite specifically as a repository medium, nor was it intended to do so. The experiment did not reveal any mechanism that should eliminate argillaceous rocks *a priori* from further consideration, but did disclose considerable phenomenological complexity in the response of argillaceous rocks to heating. This is especially true at temperatures above those at which appreciable rock-mass dehydration begins.

APPENDIX A

Estimated Field Accuracy of Measurements

The main portion of the heater experiment was started at a power level of 2.5 kW rather than the design level of 3.8 kW because of simple misinterpretation of power-meter data. After 21 days of operation, the heater power was increased to the desired level. This does not imply, however, that 3.8 kW was actually put into the rock immediately opposite the heater.

Concern about the lifespan of electrical connections in the junction section of the heater led to a decision to force air down the access pipe containing the power leads and out the one containing the thermocouple wires. This air flowed at a velocity of ~230 m/min, a volumetric flow rate of 0.03 m^3/s. Temperatures of both inlet and exhaust air were continuously measured at the surface and averaged 30°C during the main portion of the test, though there were diurnal variations of 15° to 18°C in the inlet temperature and ~3°C in the outlet. The air temperature at the bottom of the packer was also near 30°C. Temperatures within the junction section of the heater averaged 50°C. Therefore, by the time the input air was within the junction section of the heater, its temperature had increased by ~20°C from that at the bottom of the packer.

One obvious possibility is that the heating was caused by conductive heat loss out of the upper end of the heater. However, assuming a thermal conductivity of 15 W/m°C for the heater skin and elements, and 2 W/m°C for expanded vermiculite,[32] the total conductive heat loss into the junction section of the heater was estimated at only ~50 W. If this is true, the calculated rise in the temperature of the input air caused by heating in the junction section is only 1.5°C.

Before it reached the junction section, the input air went through a 0.61-m-long section tightly wrapped with fiberglass insulation. The air temperature at the bottom of this insulation rapidly increased to between 93° and 97°C after the heater was turned to full power. The stable temperature was at or slightly below 94°C, the local boiling point of water. At the end of the experiment, the entire batt of insulation was saturated with water, much like a sponge. It is therefore initially assumed that the entire mass of insulation was maintained at a constant temperature of near 90°C. With this assumption, a heat-transfer coefficient of 100 kcal/m^2-h-°C between the pipe and the inlet air, and an initial air temperature of 30°C, ~0.7 kW could have been continuously transferred from the insulation batt and inlet pipe to the inlet air before the air reached the junction box.[45] This amount of heat would increase the temperature of the inlet air by ~20°C; i.e., almost exactly to the measured temperatures inside the junction section. If the air was assumed to exit the junction section at 50°C, with the insulation a constant 90°C, then similar calculations indicate that an additional 0.4 kW of heat could be added to the exiting air by the time it reached the top of the insulation. Because the exit air at the surface was only at 30°C, however, the temperature of the exhaust air had to be buffered toward the ambient temperature of the emplacement hole along the 20-m flow path to the surface.

It thus appears possible to account for heating of the input air to measured junction-box temperatures solely by heat transfer from the fiberglass insulation to the inlet air. Three factors must be kept in mind, however. First, the heat-transfer coefficient used here, 100 kcal/m^2-h-°C, is at the upper end of the apparent range for heat transfer to flowing gases.[46] At the other extreme, 10 kcal/m^2-h-°C, only 0.07 kW would be transferred to the inlet air, and the temperature rise would only be ~2°C. Secondly, the temperature within the insulation was assumed uniform. However, the thermocouple at the bottom of the packer and ~1.3 m above the top of the insulation read only ~30°C. Therefore, there must have been either a substantial gradient across the insulation, or across the air gap between the top of the insulation and the bottom of the packer. Thirdly, that the temperature of the exit air at the surface was near 30°C required heat loss by this air between the top of the insulation and the surface. If the exiting air gave off heat over this interval, there is no reason the input air could not have been partially heated on its downward trip. If so, then the temperature of the input air as it entered the insulation-wrapped section of pipe could have been ~50°C, and the heat losses in the region of the heater quite slight.

It thus appears that a maximum uncertainty of ~1 kW remains in the thermal power input into the argillite directly from the heater during this experiment. Under the approach resulting in 1 kW estimated uncertainty, it appears that the forced cooling air served as a continuous heat sink, while the fiberglass insulation above the heater served as a continuous heat source. It remains to explain the heat-source behavior of the fiberglass.

As mentioned above, the fiberglass appeared to be a fully saturated "sponge" at the end of the experiment. In addition, the 0.005-m-deep flange at the top of the heater was filled with water. One potential mechanism for controlling temperatures at the top of the heater and for maintaining the bottom of the fiberglass at a temperature near 94°C is continuous condensation/evaporation of water.

Condensation in the fiberglass, accompanied by heat loss to inlet/exhaust air, would need to account for a heat input into the fiberglass of 1 kW at most. Given that the heat of vaporization of water is 517 cal/cm³ at 100°C, a heat release rate of 1 kW corresponds to a water condensation rate of 0.46 cm³/s of liquid water, or 1.8 x 10^{-3}m³/h. In a closed emplacement hole, this volume of water could be derived from recycling from the lower portions of the emplacement hole. After deepening of S1-1 the water condensing on the fiberglass insulation would have to have been derived from water driven out of the rock by heating.

The approximate average water-collection rate in S1-3 was ~1.4 x 10^{-4}m³H_2O/h, one order of magnitude lower than the required rate. This may have been caused by water losses in S1-1 and S1-3, or to the fact that only local refluxing occurred between the top of the heater and the fiberglass batt. It may also indicate that most heat transfer relating to heating and cooling of inlet and exhaust air was taking place above the insulation, and that heat losses in the vicinity of the heater were much less than 1 kW.

Thus considerable uncertainty remains about the amount of heat actually transferred to the rock directly from the heater in this experiment. However, since the net differential in temperature between inlet and exhaust air was generally ≤2°C, all but ~50 W of the 3.8 kW was being put into the argillite between a depth of 24.4 m and the surface.

It was stated that there were large potential errors in all measurements except temperature. Indeed, consideration of potential temperature errors caused by hole-hole shielding and differences between grout properties and argillite properties[47] indicates that the maximum credible temperature error in the grouted instrumentation holes attributable to these factors is <1°C; the estimated precision of the thermocouples is also ±1°C. Possible rotation of the PVC tubing that the thermocouples were strapped to could account for up to 0.05 m inaccuracy in placement. This is of potential concern only in the case of the innermost instrumentation hole, which is at a radius of 0.61 m. Even in this case, however, the maximum potential radial error is <10% of the nominal radius, and is not considered further.

Two thermocouples were mounted on the skin surface of the heater in an attempt to measure rock-wall temperatures. These thermocouples were placed at the end of a spring of Inconel 750 and shielded by a thin plate of Inconel 600 wrapped in gold foil. So that they would not drag against the hole wall during heater insertion, the thermocouples were held against the side of the heater by a washer consisting of a eutectic-composition alloy, $Pb_{32}Bi_{54.5}Sn_{15.5}$. This alloy has a melting point of 95°C. When the heater skin temperature reached approximately this temperature, the washers melted and the thermocouples were freed to spring out against the hole wall. Preliminary calculations[48] considering conductive heat transfer down the spring, radiative transfer to the thermocouple bead, and convective transfer along the hole wall, indicate that the two thermocouples should have read temperatures ~20°C too high. This analysis, however, ignored the major contact resistance between the spring and thermocouple sheath. In addition, the actual contact between the argillite and thermocouple bead, given the softness of the argillite, may well have been greater than assumed in the calculations. In light of these two factors, the calculated 20° error is interpreted as a maximum. At any rate, the potential errors appear to be such that the temperatures recorded by the side wall thermocouples should be maximum.

Stress changes in a soft rock such as the Eleana argillite are best measured by means of a soft-inclusion gauge. No reliable gauge of this type existed at the time of fielding; therefore, an attempt was made to modify standard Creare gauges for application in soft rocks. The Creare gauge is a vibrating wire gauge activated by a solenoid. Stress changes from the setting stress (~15 MPa) are then monitored to ~±15% accuracy by measuring frequency changes of the wire. For application to the Eleana test, however, it was felt that the setting stress, applied across the relatively small anchors of the gauges, would render stress readings meaningless. To avoid or minimize this effect, the stress gauges were first emplaced in a 3.8-cm-OD aluminum tube with 1.5-mm-thick walls. The inside of this tube was then potted to provide environmental protection for the gauges. The entire

assemblage was emplaced in the hole, and fixed in place with an expanding grout, which generated ~0.5 MPa pressure on the outside of the tube. It was not possible to calibrate this entire assemblage. At ambient temperature and for short periods of time, this approach should allow collection of reliable qualitative data. However, the thermal expansion and creep properties of the complete expanding-grout/pipe/Creare-gauge/argillite system are totally unknown. Therefore, the data from the Creare gauges must be considered only qualitative, and useful only near ambient temperature.

The vertical extensometer assemblies used in this experiment each contained four rods, and were emplaced in an open but capped hole. Anchors were set at intervals of 1.5 m in each hole, with the bottom anchor at a depth of 24.4 m, and the top one at 19.8 m. Each rod was 0.013 m in diameter and consisted of standard Invar alloy from one of the anchors up to a depth of 18.3 m. From this depth to the surface, each rod was made of stainless steel (SS304). Thermocouples were attached to the anchors at 24.4 and 19.8 m.

To be useful, extensometer data must be corrected for the thermal expansion of the extensometer rods in the heated region. Since thermocouples were emplaced only at the highest and lowest anchor positions, this cannot be done directly in the intermediate depths near 22.9 m, where it was assumed the temperatures would be greatest. The highest temperature reached at the centerplane in Hole S1-5 (a grouted thermocouple hole) was 83°C, an increase of 65°C above the ambient temperature. The highest temperatures at 24.7 and 20.1 m in this hole were 64° and 45°C, respectively. Peak temperatures recorded at the 24.4- and 19.8-m extensometer-anchor depths in S1-7 were 40° and 68°C, respectively. It is thus impossible to transfer temperatures from S1-5 to S1-7 for purposes of data reduction. Thermal convection in an open hole (S1-7) is probably responsible for the difference in the profile asymetry for the two holes. Upward convection was possible in S1-7, since the only material present in the hole (0.10-m dia) was four 0.01-m-dia rods. This type of heat transfer was prohibited in Hole S1-5 by the fact that thermocouples in this hole were grouted in place.

Some sense can be made out of relative extensometer displacements, however, especially the movement of shallower anchors relative to the anchor at 24.4 m. Considered in this way, the thermal effects at all depths less than that of the shallower anchor are presumably the same along both rods. Thus, only the thermal expansion of the extensometer rod between the two anchor positions need be removed from the data. For example, if it is assumed that the anchor at 24.4 m is at 40°C, and that the anchor at 22.9 m is at 90°C, then the maximum credible differential thermal expansion effect is only about 7.6×10^{-5} m. This value is calculated by assuming a thermal expansion coefficient of $1 \times 10^{-6}°C^{-1}$ at 90°C for the Invar rod,[49] a constant temperature differential of 50°C, and an initial differential length of 1.52 m. Since the thermal expansion coefficient chosen is the highest listed over the temperature range involved, and the temperature difference is assumed at its maximum along the entire length of rod, this calculated value should be a maximum. Note that, since the estimated thermal correction for measurements between 24.4 and 22.9 m is only about one-half the estimated instrumental error of 13×10^{-5} m, no temperature corrections are needed at these depths. Maximum thermal expansion errors between 24.4 and 19.8 m in Hole S1-7 are greater, and are calculated to be 2.4×10^{-4} m, about twice the inherent instrumental error. Thus, the vertical extensometer measurements even with the temperature uncertainties should be qualitatively correct if viewed as displacements relative to the anchor at the 24.4-m depth, and if reported relative displacements exceed $\sim 2.4 \times 10^{-4}$ m.

Measurements of volatile pressures, though greatly affected by permeability variations in the rock mass, are probably as accurate as instrumentation capability limitations allow, except for the possibility of leaks. The effects of such leaks cannot be measured, except to say that the field measurements are almost certainly minimal and of only qualitative value. The same can be said of gas transmissivity testing, since the data reduction in an inherently fractured medium must use greatly simplifying assumptions about gas flow between holes.

In summary, all measurements made as part of this test except temperature measurements in grouted thermocouple holes were accompanied by field-related uncertainties that make the data obtained necessarily qualitative.

References

[1]*The Disposal of Radioactive Waste on Land*, Report of the Committee on Waste Disposal of the Division of Earth Science, NAS Publication 519 (Washington, DC: National Academy of Sciences - National Research Council, 1957).

[2]R. G. Dosch and A. W. Lynch, *Interaction of Radionuclides with Argillite from the Eleana Formation on the Nevada Test Site*, SAND78-0893 (Albuquerque, NM: Sandia National Laboratories, 1979).

[3]T. Tamura, "Sorption Phenomena Significant in Radioactive-Waste Disposal," in *Underground Waste Management and Environmental Applications, Am Assn Petr Geol Mem.* 18, 1973, pp 318-330.

[4]I. W. Marine, "Geohydrology of Buried Triassic Basin at Savannah River Plant South Carolina," *Am Assn Petr Geol Bull.* 58:1825-1837, 1974.

[5]J. B. Droste and C. J. Vitaliano, *Geologic Report of the Maquoketa Shale, New Albany Shale, and Borden Group Rocks in the Illinois Basin on Potential Solid Waste Repository Sites*, prepared for the Office of Waste Isolation, Oak Ridge, TN, 1977.

[6]C. E. Neuzil, "Fracture Leakage in the Cretaceous Pierre Shale and Its Significance for Underground Waste Disposal" (unpubl. PhD thesis, John Hopkins University, 1980).

[7]J. L. Krumhansl, *Preliminary Results Report Conasauga Near-Surface Heater Experiment*, SAND79-0745 (Albuquerque, NM: Sandia National Laboratories, 1979).

[8]J. L. Krumhansl, *Final Report: Conasauga Near-Surface Heater Experiment*, SAND79-1855 (Albuquerque, NM: Sandia National Laboratories, 1979).

[9]E. Tassoni, "An Experiment on the Heat Transmission in a Clay Rock," pp 23-46 in *Proceedings of the NEA Workshop on the Use of Argillaceous Materials for the Isolation of Radioactive Waste*, held at Paris, France, September 10-12, 1979 (Paris, France: NEA/OECD, 1980).

[10]F. G. Poole, F. N. Houser, and P. O. Orkild, *Eleana Formation of Nevada Test Site and Vicinity, Nye County, Nevada*, USGS Prof. Paper 424-D, pp D104-D111 (Washington: Government Printing Office, 1961).

[11]F. G. Poole, "Flysch Deposits of Antler Foreland Basin, Western United States," pp58-82 in *Tectonics and Sedimentation*, Soc. Econ. Paleon. Min. Special Publ. 22, W. R. Dickinson, ed (Tulsa, OK· 1974)

[12]H. E. Simpson, J. W. Weir, and L. A. Woodward, *Inventory of Clay-Rich Bedrock and Metamorphic Derivatives in Eastern Nevada Excluding the Nevada Test Site*, USGS Open File Report 79-760 (Denver, CO: 1979).

[13]D. L. Hoover and J. N. Morrison, *Geology of the Syncline Ridge Area Related to Nuclear Waste Disposal, Nevada Test Site, Nye County, Nevada*, USGS Open-File Report, 1980.

[14]J. N. Hodson and D. L. Hoover, *Geology of the UE17e Drill Hole, Area 17, Nevada Test Site*, USGS Open-File Report USGS-1543-2, 1979.

[15]Memo from G. T. Gay to A. R. Lappin, SNL, "X-Ray Analysis of Eleana Shale," March 8, 1977.

[16]Memo from G. T. Gay to A. R. Lappin, SNL, "X-Ray Analysis of Eleana Shale," May 9, 1977.

[17]Memo from G. T. Gay to A. R. Lappin, SNL, "X-Ray Analysis of Eleana Shale," July 14, 1977.

[18]G. V. Henderson, *The Origin of Pyrophyllite - Rectorite in Shales of North Central Utah*, Utah Geol. and Mineralogical Surv. Special Studies 34, 1971.

[19]O. D. Christensen, "Metamorphism of the Manning Canyon and Chairman Formations" (PhD thesis, Stanford University, 1975).

[20]Huffman Laboratories, Inc. Analytical Report No. 4487701 to A. R. Lappin, SNL, dtd May 24, 1977 (Huffman Laboratories, Inc., 3830 High Court, P.O. Box 350, Wheat Ridge, CO 80033).

[21]R. G. Dosch, *Assessment of Potential Radionuclide Transport in Site-Specific Geologic Formations*, SAND79-2468 (Albuquerque, NM: Sandia National Laboratories, 1980).

[22]Memo from J. Husler, UNM analyst, to A. R. Lappin of SNL, "Shale Analyses," May 5, 1977.

[23]Memo from J. Husler, UNM analyst, to A. R. Lappin of SNL, "Whole-Rock Analyses, Main Heater Hole, Eleana Experiment Site, S1-1," May 24, 1978.

[24]F. J. Pettijohn, *Sedimentary Rocks*, 3rd ed. (New York: Harper and Rowe, 1975).

[25]Personal communication with L. G. Schultz, USGS.

[26]Memo from J. Husler, UNM analyst, to A. R. Lappin of SNL, "Trace Element Analysis, PPM," June 25, 1977.

[27]Memo from J. Husler, UNM analyst, to A. R. Lappin of SNL, "Trace Element Analyses, Main Heater Hole, Eleana Experiment Site, S1-1 (PPM)," May 22, 1978.

[28]K. B. Krauskopf, *Introduction to Geochemistry* (New York: McGraw-Hill, 1967).

[29]C. E. Weaver and K. C. Beck, *Clay-Water Diagenesis During Burial: How Mud Becomes Gneiss*, Geol Soc Am Spec Paper 134, 1971.

[30]L. A. Anderson, R. J. Bisdorf, and D. R. Schoenthaler, *Resistivity Sounding Investigation by the Schlumberger Method in the Syncline Ridge Area, Nevada Test Site, Nevada*, USGS Open File Report 80-466, 1980.

[31]B. J. Murphy, M. Charnack, and D. L. Hoover, *Engineering Geology of the Eleana Heating Experiment Site, Area 17, Nevada Test Site*, USGS Open-File Report USGS-464265 (in press).

[32]D. K. Gartling, *COYOTE—A Finite Element Computer Program for Nonlinear Heat Conduction Problems*, SAND77-1332 (Albuquerque, NM: Sandia National Laboratories, 1978).

[33]G. R. Hadley and J. E. R. Turner, Jr., *Evaporation Water Loss from Welded Tuff*, SAND80-0201 (Albuquerque, NM: Sandia National Laboratories, 1980).

[34]D. F. McVey, A. R. Lappin, and R. K. Thomas, "Test Results and Supporting Analysis of a Near-Surface Heater Experiment in the Eleana Argillite," pp93-110 in *Proceedings of the Use of Argillaceous Materials for the Isolation of Radioactive Waste*, held at Paris, France, September 10-12, 1979 (Paris, France: NEA/OECD, 1980).

[35]Memo from D. F. McVey of SNL to Distribution, "Thermal Predictions—Large-Scale Eleana Heater Test," April 13, 1978.

[36]Memo from D. F. McVey to A. R. Lappin, SNL, "Revised Thermal Predictions—Large-Scale Eleana Heater Test," January 22, 1979.

[37]K. J. Bathe, ADINA, *A Finite Element Program for Automatic Dynamic Incremental Nonlinear Analysis*, MIT Report 82448-1, 1977.

[38]A. R. Lappin and W. A. Olsson, "Material Properties of Eleana Argillite—Extrapolation to Other Argillaceous Rocks, and Implications for Waste Management," pp75-91 in *Proceedings of the Use of Argillaceous Materials for the Isolation of Radioactive Waste*, held at Paris, France, September 10-12, 1979 (Paris, France: NEA/OECD, 1980).

[39]W. A. Braddock and M. Machette, *Experimental Deformation of Pierre Shale*, Document AFGL-TR-76-0086 (Hanscom AFB, MA: Air Force Geophysical Laboratory, Air Force Systems Command, USAF, 1976).

[40]D. F. McVey, R. K. Thomas, and A. R. Lappin, *Small Scale Heater Tests in Argillite of the Eleana Formation at the Nevada Test Site*, SAND79-0344 (Albuquerque, NM: Sandia National Laboratories, 1979).

[41]D. F. McVey, R. K. Thomas, and A. R. Lappin, *Farfield Thermomechanical Response of Argillaceous Rock to Emplacement of a Nuclear-Waste Repository*, SAND79-2230 (Albuquerque, NM: Sandia National Laboratories, 1980).

[42]C. E. Weaver, *Geothermal Alteration of Clay Minerals and Shales: Diagenesis*, ONWI-21, 1979.

[43]Memo from J. Husler, UNM analyst, to A. R. Lappin of SNL, "Chemical Analyses of Posttest Eleana Samples," September 14, 1979.

[44]Memo from J. W. Braithwaite and W. L. Larson of SNL to Distribution, "Metallurgical Examination of Metals Used in Eleana Heater Experiment," June 1, 1979.

[45]Memo from A. R. Lappin of SNL to Distribution, "Junction-Section Heat Losses of Eleana Heater Due to Forced Cooling," July 26, 1978.

[46]R. B. Bird, W. E. Stewart, and E. N. Lightfoot, *Transport Phenomena* (New York: John Wiley and Sons, Inc., 1960).

[47]Memo from D. F. McVey of SNL to J. F. Cuderman of SNL, "Influence of Grout Thermal Conductivity and Density on Measured Temperatures in Nevada Eleana Shale Thermal Experiment," July 29, 1977.

[48]Memo from B. M. Bulmer of SNL to D. F. McVey of SNL, "Eleana Heat-Transfer Experiment: Thermocouple Analysis," November 30, 1977.

[49]Y. S. Touloukian, et al, *Thermophysical Properties of Matter*, vol 12 of *Thermal Expansion (of) Metallic Elements and Alloys* (New York: IFI/Plenum, 1975).

DISTRIBUTION:

US Department of Energy
Assistant Secretary
for Defense Programs
Mail Stop SF-066
Washington, DC 20545
Attn: D. C. Sewell (DP-1)

US Department of Energy
Assistant Secretary Nuclear Energy
Mail Stop 6E-09S
Washington, DC 20545
Attn: G. W. Cunningham (NE-1)

US Department of Energy (9)
Office of Nuclear Waste Management
Mail Stop B-107
Germantown, MD 20767
Attn: S. Meyers (NE-30)
R. G. Romatowski (NE-30)
C. A. Heath (NE-330)
D. L. Vieth (NE-332)
R. Stein (NE-330)
C. R. Cooley (NE-330)
M. W. Frei (NE-332)
G. P. Dix (EV-12)
C. D. Newton (NE-30)

US Department of Energy (2)
Richland Operations Office
Post Office Box 550
Richland, WA 99352
Attn: F. Standerfer
D. J. Squires

US Department of Energy
Albuquerque Operations Office
Post Office Box 5400
Albuquerque, NM 87115
Attn: D. T. Schueler, Jr.

US Department of Energy
San Francisco Operations Office
1333 Broadway, Wells Fargo Bldg.
Oakland, CA 94612
Attn: L. Lanni

Rockwell International
Atomics International Division
Rockwell Hanford Operations
Richland, WA 99352
Attn: R. Deju
B. Dietz

US Department of Energy (27)
Nevada Operations Office
Post Office Box 14100
Las Vegas, NV 89114
Attn: M. E. Gates
R. W. Taft
R. W. Newman
J. B. Cotter
M. P. Kunich
H. L. Melancon
C. P. Bromley
R. H. Richards
F. C. Hood
A. J. Roberts
R. M. Nelson
D. F. Miller
P. J. Mudra
R. H. Marks, CP-1, M/S 210
S. R. Elliott
B. W. Church
T. H. Blankenship
R. R. Loux (10)

US Department of Energy (3)
NTS Support Office
Post Office Box 435
Mercury, NV 89023
Attn: J. H. Dryden, M/S 701
F. Huckabee, M/S 701
L. P. Skousen, M/S 701

US Department of Energy
DOE-IX
Director of External Affairs
333 Market Street, 7th Floor
San Francisco, CA 94105
Attn: D. J. Cook

US Department of Energy
National Program Office
505 King Avenue
Columbus, OH 43201
Attn: J. O. Neff

Nuclear Regulatory Commission (3)
Washington, DC 20555
Attn: J. C. Malaro, M/S SS-674
R. Boyle, M/S P-522
D. Alexander, M/S 905SS

DISTRIBUTION (cont):

Holmes & Narver, Inc.
Post Office Box 14340
Las Vegas, NV 89114
Attn: A. E. Gurrola, M/S 158

Lawrence Livermore National Laboratory (8)
University of California
Post Office Box 808
Livermore, CA 94550
Attn: L. D. Ramspott, L-204
A. Holzer, L-209
L. B. Ballou, L-204
R. L. Wagner, L-1
K. Street, L-209
W. C. Patrick, L-204
A. B. Miller, L-204
D. J. Isherwood, L-224

Los Alamos National Laboratory (5)
University of California
Post Office Box 1663
Los Alamos, NM 87545
Attn: K. Wolfsberg, M/S 514
L. S. Germain, M/S 570
L. Lanham, M/S 755
B. R. Erdal, M/S 514
J. R. Smyth, M/S 978

Westinghouse (8)
Post Office Box 708
Mercury, NV 89023
Attn: A. R. Hakl, M/S 703

Westinghouse - AESD (11)
Post Office Box 10864
Pittsburgh, PA 15236
Attn: J. B. Wright (6)
W. R. Morris
T. E. Cross
R. J. Bahorich
C. R. Bolmgren
W. A. Henninger

Nuclear Fuel Cycle Research
University of Arizona
Tucson, AZ 85721
Attn: J. G. McCray

US Geological Survey (3)
National Center
Restor, VA 22092
Attn: G. D. DeBuchananne, M/S 410
P. R. Stevens, M/S 410
D. B. Stewart, M/S 959

US Geological Survey (3)
Post Office Box 25046
Federal Center
Denver, CO 80301
Attn: W. S. Twenhofel, M/S 954
G. L. Dixon, M/S 954
D. L. Hoover, M/S 954

Geologic Society of America
3300 Penrose Place
Boulder, CO 80301
Attn: J. C. Frye

Kansas Geological Survey
University of Kansas
Lawrence, KS 66044
Attn: W. W. Hambleton

Battelle (17)
Office of Nuclear Waste Isolation
505 King Avenue
Columbus, OH 43201
Attn: N. E. Carter
S. C. Matthews
W. E. Newcomb
W. M. Hewitt
R. J. Hall
S. J. Basham
G. E. Raines
N. J. Hubbard
J. E. Monsees
J. A. Carr
ONWI Library (5)
R. A. Robinson
W. A. Carbiener

State of Nevada
Capitol Complex
Carson City, NV 89710
Attn: R. Hill,
State Planning Coordinator

Fenix & Scisson, Inc.
Post Office Box 498
Mercury, NV 89023
Attn: F. D. Waltman, M/S 940

State of Nevada
Capitol Complex
Carson City, NV 89710
Attn: N. Clark,
Department of Energy

DISTRIBUTION (cont):

Western Region Library
No. 3 Embarcardero Center
San Francisco, CA 94111
Attn: Woodward-Clyde Consultants

Department of Chemistry
Idaho State University
Pocatello, ID 83201
Attn: J. L. Thompson

Holmes & Narver, Inc.
Post Office Box I
Mercury, NV 89023
Attn: G. E. Christensen, M/S 605

John A. Blume Engineers
Sheraton Palace Hotel
130 Jessie Street
San Francisco, CA 94105
Attn: P. Yanev

Harvard University
Department of Earth Sciences
Cambridge, MA 02138
Attn: R. Siever

Department of Earth Sciences
Dartmouth College
Hanover, NH 03755
Attn: J. Lyons

International Atomic Energy Agency
Division of Nuclear Power & Reactors
Karntner Ring 11
Post Office Box 590, A-1011
Vienna, Austria
Attn: J. P. Colton

Fenix & Scisson, Inc.
Post Office Box 15408
Las Vegas, NV 89114
Attn: J. A. Cross, M/S 514

Princeton University
Department of Civil Engineering
Princeton, NJ 07540
Attn: G. Pinder

California Energy Resources
Conservation & Development
Commission
1111 Howe Avenue
Sacramento, CA 95825
Attn: A. Soinski

University of California
Lawrence Berkeley Laboratory
Energy & Environment Division
Berkeley, CA 94720
Attn: P. Witherspoon

Hanford Engineering Development
Laboratory
Post Office Box 1970
Richland, WA 99352
Attn: D. Cantley

Arthur D. Little, Inc.
Acorn Park
Cambridge, MA 02140
Attn: C. R. Hadlock

Brown University
Department of Geological
Sciences
Providence, RI 02912
Attn: B. Giletti

Texas A&M University
Center for Tectonophysics
College Station, TX 77840
Attn: J. Handin

Law Engineering Testing Co.
2749 Delk Road, S.E.
Marietta, GA 30067
Attn: B. Woodward

Subcommittee on Energy
Research & Production
Room B-374
Rayburn House Office Bldg.
Washington, DC 20575
Attn: S. Lanes, Staff Director

Bureau of Radiation Control
Department of Health and Environment
Forbes Field
Topeka, KS 66620
Attn: G. W. Allen, Director

State of Connecticut
Energy Research and Policy
80 Washington Street
Hartford, CT 06115
Attn: F. N. Brenneman

DISTRIBUTION (cont):

Executive Office
Lansing, MI 48909
Attn: W. C. Taylor,
Science Advisor

Director for Policy and Planning
Room 300, 325 West Adams Street
Springfield, IL 62706
Attn: A. Liberatore

Nuclear Projects Coordinator
Nuclear Energy Division
Post Office Box 14690
Baton Rouge, LA 70808
Attn: L. Hall Bohlinger

Oregon Department of Energy
Labor & Industries Bldg.
Room 111
Salem, OR 97310
Attn: D. W. Godard

Radiation Protection Division
1000 Northeast 10th Street
Post Office Box 53551
Oklahoma City, OK 73152
Attn: R. L. Craig, Director

Reynolds Electrical & Eng. Co., Inc. (7)
Post Office Box 14400
Las Vegas, NV 89114
Attn: H. D. Cunningham, M/S 555
W. G. Flangas, M/S 615
G. W. Adair, M/S 154
V. M. Milligan, M/S 765
C. W. Dunnam, M/S 745
R. L. Powell, M/S 634
R. B. Land, M/S 585

Radiation Health Information Project
Environmental Policy Inst.
317 Pennsylvania Ave., S.E.
Washington, DC 20003
Attn: E. Walters

Nuclear Safety Associates, Inc.
5101 River Road
Bethesda, MD 20016
Attn: J. A. Lieberman

Federal Agency Relations
1050 17th St., N.W.
Washington, DC 20036
Attn: O. H. Davis, Director

Environmental Program Supervisor
903 Ninth Street Office Bldg.
Richmond, VA 23219
Attn: K. J. Buttleman

Energy Administration
Department of Natural Resources
Tawes State Office Bldg.
Annapolic, MD 21401
Attn: P. Massicot, Acting Director

State of Ohio Environmental
Protection Agency
Box 1049, 361 E. Broad St.
Columbus, OH 43216
Attn: J. F. McAvoy, Director

State of Connecticut
House of Representatives
One Hundred and Sixth District
24 Rock Ridge Road
Newton, CT 06470
Attn: J. W. Anderson

Missouri Department of Natural Resources
Post Office Box 176
Jefferson City, MO 65102
Attn: T. D. Davis

Mississippi Department of Natural Resources
Suite 228, Barefield Complex
455 North Lamar Street
Jackson, MS 39201
Attn: P. T. Bankston

Tennessee Energy Authority
Suite 708 Capitol Blvd. Bldg.
Nashville, TN 37219
Attn: J. A. Thomas, Associate Director

Council Member
374 South Rock River Drive
Berea, OH 44017
Attn: G. A. Brown

DISTRIBUTION (cont):

Public Law Utilities Group
One American Place, Suite 1601
Baton Rouge, LA 70825
Attn: D. Falkenheier,
Assistant Director

Associate Dean for Research
Georgia Institute of Technology
Atlanta, GA 30332
Attn: R. Williams

Fenix & Scisson, Inc.
Post Office Box 498
Mercury, NV 89023
Attn: D. A. Robins, M/S 940

Reynolds Electrical & Engineering Co., Inc.
Post Office Box 14400
Las Vegas, NV 89114
Attn: E. H. Weintraub, M/S 625

US Department of Energy (2)
Division of Waste Isolation
Germantown, MD 20767
Attn: J. W. Rowen, (DP-342)
M. E. Langston, (ME-512), M/S B-107

Energy Facility Site
Evaluation Council
820 East Fifth Avenue
Olympia, WA 98504
Attn: N. D. Lewis

University of Texas at Austin
University Station, Box X
Austin, TX 78712
Attn: E. G. Wermund

Department for Human Resources
Commonwealth of Kentucky
Frankfort, KY 40601
Attn: R. M. Fry

Office of Energy Resources
73 Tremont Street
Boston, MA 02108
Attn: L. Morgenstern

Department of Environmental Regulation
Twin Towers Office Bldg.
2600 Blair Stone Road
Tallahassee, FL 32301
Attn: D. S. Kell

Holmes & Narver
Post Office Box I
Mercury, NV 89023
Attn: V. L. Angell, M/S 605

Westinghouse
Post Office Box 708
Mercury, NV 89023
Attn: R. L. Malloy, M/S 703

EG&G, Inc.
Post Office Box 295
Mercury, NV 89023
Attn: W. C. Roper, M/S 570/N24

Office of Nuclear Waste Isolation
505 King Avenue
Columbus, OH 43201
Attn: M. J. Golis

Hanford Engineering
Development Laboratory
Post Office Box 1970
Richland, WA 99352
Attn: D. L. Garland

Rockwell Hanford Operations
Post Office Box 800
Richland, WA 99352
Attn: D. A. Turner

Westinghouse Electric Corp.
Post Office Box 40039
Albuquerque, NM 87106
Attn: D. I. Hulbert

Oak Ridge National Laboratories
Post Office Box X
Oak Ridge, TN 37830
Attn: H. C. Claiborne

Rockwell Hanford Operations
Energy Systems Group
Post Office Box 800
Richland, WA 99352
Attn: K. R. Hoopingarner,
Manager, Master Planning

Battelle Pacific Northwest Laboratory
Post Office Box 999
Richland, WA 99352
Attn: J. L. McElroy

DISTRIBUTION (cont):

RE/SPEC, Inc.
Post Office Box 725
Rapid City, SD 57709
Attn: J. D. Osnes

Science Applications, Inc.
Post Office Box 843
Oak Ridge, TN 37830
Attn: L. D. Rickertsen

E. I. DuPont de Nemours & Company
Savannah River Laboratory
Aiken, SC 29801
Attn: N. E. Bibler

US Department of Energy
Nuclear Environmental Application Branch
Mail Station E-201 (Gtn)
Washington, DC 20545
Attn: R. W. Barber, Acting Chief

Gesellschaft fur Strahlen-und
Umweltforschung MBH Munchen
Institut fur Tieflagerung
3392 Clausthal-Zellerfeld
Berliner Strasse 2
Federal Republic of Germany
Attn: K. Kuhn

Hahn-Meitner-Institut fur Kernforschung
Glienicker Strasse 100
1000 Berlin 39
Federal Republic of Germany
Attn: K. Eckart Maass

Bundesanstalt fur Geowissenschaften
und Rohstoffe
Postfach 510 153
3000 Hannover 51
Federal Republic of Germany
Attn: M. Langer

Kernforschung Karlsruhe
Postfach 3640
7500 Karlsruhe
Federal Republic of Germany
Attn: R. Kraemer

Physikalische-Technische
Bundesanstalt
Bundesalle 100, 3300 Braunschweig
Federal Republic of Germany
Attn: H. Rothemeyer

Bundesministerium fur Forschung
und Technologie
Postfach 200 706
5300 Bonn 2
Federal Republic of Germany
Attn: Rolf-Peter Randl

Georgia Institute of Technology
School of Nuclear Engineering
Atlanta, GA 30332
Attn: M. Carter

1417 F. W. Muller
1417 G. F. Rudolfo
1762 M. R. Zimmerman
4413 N. R. Ortiz
4500 E. H. Beckner
4510 W. O. Weart
4530 R. W. Lynch
4537 L. D. Tyler (10)
4537 A. R. Lappin (50)
4538 R. C. Lincoln
4540 M. L. Kramm
4550 R. M. Jefferson
5510 D. B. Hayes
5511 J. W. Nunziato
5512 D. F. McVey (10)
5521 L. W. Davison
5521 R. K. Thomas (10)
5532 B. M. Butcher
5532 W. A. Olsson
5541 W. C. Luth
5541 J. L. Krumhansl
8214 M. A. Pound
3141 L. J. Erickson (5)
3151 W. L. Garner (3)
For DOE/TIC (Unlimited Release)
DOE/TIC (25) (C. H. Dalin, 3154-3)

Org.	Bldg.	Name	Rec'd by *	Org.	Bldg.	Name	Rec'd by *